Accepted for publication in Composite Structures, Vol. 200, 15 Sept. 2018, Pages 781-79
https://doi.org/10.1016/j.compstruct.2018.05.078

Multiscale Surrogate Modelling of the Elastic Response of Thick Composite Structures with embedded defects and features

Bassam El Said and Stephen R. Hallett

University of Bristol, UK

Abstract

This paper presents a multiscale modelling approach for thick composite structures containing internal defects and features. The proposed approach was developed using a surrogate model to represent the composite response on the meso-scale. A set of Representative Volume Element (RVE) models under periodic boundary conditions were used to sample the response at specified locations across the composite design space. As an example of its application, wrinkle defects of various severities were introduced to the RVE models to assess the defect contribution to the composite response. The homogenized responses from the meso-scale RVE models were then used as input to the surrogate model. To link the macro and meso scales, a set of 3D lamination parameters representing the composite layup were developed. A surrogate model using the 3D lamination parameters and the defect severity as input was built to link the macro-model to the meso-scale responses. The proposed multi-scale approach was verified against a set of high fidelity models with different levels of wrinkle defect severity. Good agreement was found between the new multi-scale approach and the more computationally expensive high-fidelity models.

1. Introduction

A main advantage of laminated fibre reinforced composite materials for structural applications comes from the ability to select the fibre orientation on a layer by layer basis, which leads to highly optimisable configurations. By carefully selecting the orientations, the stress and load paths within a structure can be tailored to achieve the desired performance [1, 2]. Additionally, enhanced damage tolerance can be built into the structure. Selected damage modes can be suppressed for the benefit of more favourable ones [3, 4]. However, this flexibility comes at the cost of a considerably more complex internal material architecture. The external geometric features of the structures such as curves, tapers, holes, and notches lead to a more complex internal architecture. For example, the presence of a feature such as ply drops to achieve a change

in thickness can lead to the onset of delamination [5] as well as promoting fibre waviness. Manufacturing methods such as Automated Fibre Placement (AFP) are associated with introducing internal defects in the form of gaps and overlaps [6]. As AFP becomes more prominent in composite structures manufacturing, the need arises for efficient modelling techniques to predict the effect of internal features on the macro-scale behaviour [7]. The existence of these internal defects and features can change both the stiffness and strength of as-manufactured composites from that of an ideal material. In this paper, the distinction is made between a defect and a feature within the composite laminate. Defects are an unintended manufacturing variability from the design intent, while features are an essential part of the composite design and manufacture process, such as the case of a ply drop in a tapered section. From a structural point, both types of internal feature can impact the mechanical performance and can be modelled using the same approaches. Internal defects and features which change the local fibre orientation lead to a localized reduction in stiffness. Additionally, they can act as damage initiators or interact with damage progression, thus reducing the composite strength [8, 9].

To deal with the complexities associated with the presence of internal defects and features in composite structures, two main scales are defined, the meso-scale and the macro-scale. The meso-scale is at the level where the individual plies and their orientations are visible. Also, at this scale defects such as waviness, gaps and overlaps are defined. The geometry of the structure is defined at the macro-scale, as well as the applied loads and boundary conditions. At this scale, the internal features are not defined explicitly. To deal with these two substantially different length scales, multi-scale modelling techniques have been proposed in the literature [10-12]. One of the main challenges for multiscale modelling of composites is representing the effect of the meso-scale features in a macro-scale model. This problem becomes more challenging when macro-scale models are used for design space exploration. In the earlier phases of the design process, engineers are concerned with finding optimum layups and optimum locations for necessary features such as ply drops. During this phase, a multitude of design options should be modelled and evaluated. This process becomes computationally intensive if the defects and features are described explicitly in the macro model. Here, a novel multiscale model approach is presented to handle the complexities associated with modelling this category of composite structures. This paper will focus on the stiffness response, while additional work will be necessary to address damage initiation and progression from such localised features.

The proposed modelling approach consists of three main components: a database of Representative Volume Element (RVE) models, a computational homogenization module and a surrogate model. The RVE models are at the meso-scale and can contain any combination of defect and feature, solved under periodic boundary conditions for multiple load cases. The computational homogenization module calculates the effective homogenized response of the RVE models. Finally, the surrogate model is based on a database of RVE responses and is linked to the macro-scale model, thus removing the need to run RVE models in parallel with the macro simulation. This significantly reduces the model computational cost. A schematic of the proposed modelling approach is shown in Figure 1.

One of the techniques that is commonly used in design space exploration for composite materials is lamination parameters [13-15]. Lamination parameters are derived from Classical Laminate Analysis (CLA). In this approach, the stiffness tensor of a composite layup is divided into two sets of components. The material components are called the material invariants, and the lamination parameters are based on the orientations of the plies and staking sequence. The lamination parameters approach has been used to optimize the behaviour of composite structures to achieve specific behaviour for enhanced buckling performance [16-19], aeroelastic tailoring [20-22] and stiffness tailoring [16, 23-27]. In these CLA based approaches, lamination parameters were used to sample the layup design space in a methodical manner. High fidelity or analytical models were used to calculate the layup behaviour at specific design points described by a set of lamination parameters. Using the knowledge of the response at these points, surrogate models can be built to give a continuous representation of the response for the complete design space. Because the lamination parameters are used to represent the layup contribution in the surrogate model, the behaviour of the macro-scale structure can be predicted from the knowledge of the local lamination parameters across the structure. However, since the derivation of these lamination parameters assumes plate kinematics at the macro-scale they are not suitable for modelling the types of thick structures under consideration here. For these, 3D solid finite element formulations are required, to give adequate representation of through thickness deformations, which are lacking in plate kinematics. A new approach is therefore required, able to predict a full 3D stiffness tensor, including the through thickness components. The following sections of this paper are dedicated to the construction of the various multiscale approach components as well as developing the necessary 3D lamination parameters.

Accepted for publication in Composite Structures, Vol. 200, 15 Sept. 2018, Pages 781-79
https://doi.org/10.1016/j.compstruct.2018.05.078

2. Representative Volume Element Models

Periodic homogenization has been widely used to predict the performance of composite materials [28-34] with a repeating unit cell type micro or meso-structure. To predict the performance of a given composite, an RVE of the material meso-structure is constructed and solved under Periodic Boundary Conditions (PBC). The RVE model represents the performance of an infinitely repeating sub-set of the full material volume. In this work, RVE models of a small volume of composite material containing a defect are solved as fully periodic in all 3 directions. Consequently, the model external surface, edge and corner displacements are all linked using the PBCs. For this work, the RVE models have been implemented in the commercial FE solver ABAQUS/standard using *Equation keyword to link the nodes on the RVE surfaces individually. An average strain can be applied to a given unit cell by introducing a displacement control to the PBC equations. By choosing which RVE face is under a prescribed displacement and the direction of this displacement, any combination of loading conditions can be modelled. These unit cell models are built on the meso-scale and give a detailed image of the stress / strain state on that scale. To calculate the equivalent response of an RVE model on the macro-scale, a link has to be established between the two scales. This link can be created by enforcing energy equivalence between the meso/macro models. The resulting relation is given in Equation (1):

$$\langle \sigma(X,y) : \varepsilon(X,y) \rangle_{RVE} = \Sigma(X) : E(X) \tag{1}$$

where X is the macro-scale coordinate system, y is the meso-scale coordinate system, $\sigma(X,y)$ and $\varepsilon(X,y)$ are the meso-scale stresses and strains, $\Sigma(X)$ and $E(X)$ are the macro-scale stresses and strains. In the case of an RVE model under a prescribed average strain, an effective stiffness tensor can be calculated with the knowledge of the macro stress on the RVE. The average macro stresses can be calculated using volume integration over the RVE following Equation (2).

$$\Sigma(X) = \frac{1}{V}\int \sigma(X,y)dV \tag{2}$$

Once the macro stresses are calculated an effective stiffness tensor can be calculated with the knowledge of the applied strains for each load case following Equation (3).

$$Q^H(X) = \frac{\Sigma(X)}{E(X)} \tag{3}$$

The stiffness tensor Q^H is a fourth order tensor and can be assembled from 6 load cases. The most convenient load cases are 3 pure axial cases and 3 pure shear cases. Different defects and features can be introduced to an RVE model to predict the effect of these defects on the material response. Here, wrinkle type defects were chosen to demonstrate the proposed modelling approach. However, other defect types can also be included in a similar manner. A wrinkle severity will be defined by the maximum misalignment angle following the convention described by Mukhopadhyay et al [8] . Figure 2 shows a schematic of the wrinkle definition used in this paper. Figure 3 shows an example of a single RVE model with a wrinkle under different loading conditions. The RVE size has been set equal to the period of the defect size. This was done to calculate the maximum defect impact on the response of an RVE. When the homogenised results are used on the macro-scale, the defect severity can be scaled by comparing the defect period to the macro-element RVE size.

In practice, using periodic homogenization to solve multi-scale problems entails a prior knowledge of the layup and defect density/severity. For structures with defects and features this requires solving a large number of different RVE models. Since building and solving these models can be computationally expensive this approach has limited applicability as a tool for design space exploration. A different approach is needed to expand the knowledge of the response from a discrete set of RVE models to represent the entire design space. In the next section, an approach combining periodic homogenization with surrogate modelling will be presented. This approach strikes a good balance between computational efficiency and accuracy.

3. Surrogate Modelling for Composites with Internal Defects

3.1 Lamination Parameters in a 3D Continuum

Several surrogate modelling techniques have been used in engineering applications such as Response Surface Methodology (RSM) [35], Kriging [36] and Artificial Neural Network (ANN) [37]. In these techniques, mathematical models are built to represent a continuous response everywhere across the design space from only the knowledge of a discrete set of responses. To develop a surrogate model for stiffness response of thick composites, the parameters controlling this response have to be identified. As mentioned in previous sections, lamination parameters are commonly used to represent the effect of ply orientation in surrogate models of composites. However, the conventional lamination parameters, which are derived from CLA, are not sufficient for modelling thick

composites. Instead, a new set of lamination parameters must be derived. This derivation starts from the stiffness tensor of a single composite ply defined in local material coordinates, which is given by:

$$\begin{Bmatrix}\sigma_1\\ \sigma_2\\ \sigma_3\\ \sigma_4\\ \sigma_5\\ \sigma_6\end{Bmatrix} = \begin{bmatrix} Q_{11} & Q_{12} & Q_{13} & 0 & 0 & 0 \\ & Q_{22} & Q_{23} & 0 & 0 & 0 \\ & & Q_{33} & 0 & 0 & 0 \\ & & & Q_{44} & 0 & 0 \\ & & & & Q_{55} & 0 \\ Sym & & & & & Q_{66} \end{bmatrix} \begin{Bmatrix}\varepsilon_1\\ \varepsilon_2\\ \varepsilon_3\\ \varepsilon_4\\ \varepsilon_5\\ \varepsilon_6\end{Bmatrix} \tag{3}$$

The ply stiffness tensor defined in the local material coordinates can be described in global coordinates using a rotation around the stack axis (Z). A rotation matrix linking the local coordinate system (1,2,3) to the RVE main coordinate (X, Y, Z) is given by:

$$\mathrm{T} = \begin{bmatrix} l_x^2 & l_y^2 & 0 & l_x l_y & 0 & 0 \\ r_x^2 & r_y^2 & 0 & r_x r_y & 0 & 0 \\ 0 & 0 & 1 & 0 & 0 & 0 \\ 2l_x r_x & 2l_y r_y & 0 & l_x r_y + l_y r_x & 0 & 0 \\ 0 & 0 & 0 & 0 & l_x & l_y \\ 0 & 0 & 0 & 0 & r_x & r_y \end{bmatrix} \tag{4}$$

The rotation matrix shown here is defined in a direction cosines notation. l_x, l_y , r_x and r_y are the direction cosines linking the ply material axis (1 and 2) with the RVE axis (X and Y) respectively. Figure 4 shows the relation between the direction cosines and the fibre orientation in a single ply which is defined by the angle θ . By applying this rotation, the stiffness tensor (Q^X) of a single ply given in RVE coordinates can is written as:

$$Q^X = T^T . Q^x . T \tag{5}$$

Which yields Q^X as:

(6)

Accepted for publication in Composite Structures, Vol. 200, 15 Sept. 2018, Pages 781-79
https://doi.org/10.1016/j.compstruct.2018.05.078

$$Q^X = \begin{bmatrix} Q_{XXXX} & Q_{XXYY} & Q_{XXZZ} & Q_{XXXY} & 0 & 0 \\ & Q_{YYYY} & Q_{YYZZ} & Q_{YYXY} & 0 & 0 \\ & & Q_{ZZZZ} & Q_{ZZXY} & 0 & 0 \\ & & & Q_{XYXY} & 0 & 0 \\ & & & & Q_{XZXZ} & Q_{XZYZ} \\ Sym & & & & & Q_{YZYZ} \end{bmatrix}$$

Using trigonometric identities and the knowledge that the fibre direction in a ply can be defined by only one angle, the terms r_x and r_y can be eliminated from the stiffness tensor. The stiffness tensor in RVE coordinates can be defined on a term by term basis as follows.

Axial X Stiffness:

$$Q_{XXXX} = (Q_{11} - 2Q_{12} + Q_{22} - 4Q_{44}).l_x^4 + (2Q_{12} - 2Q_{22} + 4Q_{44}).l_x^2 + Q_{22} \quad (7)$$

Axial X/ axial Y stiffness coupling term:

$$Q_{XXYY} = (-Q_{11} + 2Q_{12} - Q_{22} + 4Q_{44}).l_x^4 + (Q_{11} - 2Q_{12} + Q_{22} - 4Q_{44}).l_x^2 + Q_{12} \quad (8)$$

Axial X / axial Z stiffness coupling term:

$$Q_{XXZZ} = (Q_{13} - Q_{23}).l_x^2 + Q_{23} \quad (9)$$

Axial X / Shear XY stiffness coupling term:

$$Q_{XXXY} = (Q_{11} - 2Q_{12} + Q_{22} - 4Q_{44}).l_x^3 l_y + (Q_{12} - Q_{22} + 2Q_{44}).l_x l_y \quad (10)$$

Axial Y Stiffness:

$$Q_{YYYY} = (Q_{11} - 2Q_{12} + Q_{22} - 4Q_{44}).l_x^4 + (-2Q_{11} + 2Q_{12} + 4Q_{44}).l_x^2 + Q_{11} \quad (11)$$

Axial Y / axial Z stiffness coupling term:

$$Q_{YYZZ} = (-Q_{13} + Q_{23}).l_x^2 + Q_{13} \quad (12)$$

Axial Y / shear XY stiffness coupling term:

$$Q_{YYXY} = (-Q_{11} + 2Q_{12} - Q_{22} + 4Q_{44}).l_x^3 l_y + (Q_{11} - Q_{12} - 2Q_{44}).l_x l_y \quad (13)$$

Axial Z Stiffness:

$$Q_{ZZZZ} = Q_{33} \quad (14)$$

Axial Z / shear XY stiffness coupling term:

$$Q_{ZZXY} = l_x l_y (Q_{13} - Q_{23}) \quad (15)$$

XY Shear Stiffness:

$$Q_{XYXY} = (-Q_{11} + 2Q_{12} - Q_{22} + 4Q_{44}).l_x^4 + (Q_{11} - 2Q_{12} + Q_{22} - 4Q_{44}).l_x^2 + Q_{44} \quad (16)$$

XZ Shear Stiffness:

$$Q_{XZXZ} = (Q_{55} - Q_{66}).l_x^2 + Q_{66} \quad (17)$$

XZ shear / YZ shear coupling term:

$$Q_{XZYZ} = (Q_{55} - Q_{66}).l_x l_y \quad (18)$$

YZ Shear Stiffness:

$$Q_{YZYZ} = (-Q_{55} + Q_{66}).l_x^2 + Q_{55} \quad (19)$$

The direction cosines l_x and l_y are related to the ply orientation following:

$$l_x = cos(\theta) \quad (20)$$
$$l_y = cos(\pi - \theta)$$

For a composite layup with multiple orientations through the thickness, kinematic homogenization can be applied to find the equivalent elastic stiffness tensor. Kinematic

Accepted for publication in Composite Structures, Vol. 200, 15 Sept. 2018, Pages 781-79
https://doi.org/10.1016/j.compstruct.2018.05.078

homogenization assumes constant strain on the unit cell boundaries. By applying energy equivalence between meso and macro scales the homogenized stiffness tensor is given by:

$$Q^H = \frac{1}{V}\int Q^X dV \tag{21}$$

Assuming constant material properties through the composite thickness, the kinematic homogenization can be reduced to an integration over the thickness. The homogenized stiffness tensor then can be described in terms of material invariants and lamination parameters. The material invariants U_1 to U_{12} are dependent on the material properties and are constant across the unit cells. These invariants are given by:

$$U_1 = (Q_{11} - 2Q_{12} + Q_{22} - 4Q_{44}) \qquad U_2 = (2Q_{12} - 2Q_{22} + 4Q_{44}) \qquad U_3 = (Q_{13} - Q_{23})$$

$$U_4 = Q_{13} \qquad U_5 = Q_{22} \qquad U_6 = Q_{12}$$

$$U_7 = Q_{23} \qquad U_8 = Q_{33} \qquad U_9 = Q_{44}$$

$$U_{10} = Q_{66} \qquad U_{11} = Q_{55} \qquad U_{12} = (Q_{55} - Q_{66})$$

In conjunction with the material invariants, the lamination parameters can be described in terms of the integral of the direction cosines through the thickness and are given by:

$$\zeta = \begin{cases} \zeta_1 = \frac{1}{h}\int_{-h/2}^{h/2} l_x^4\, dt \\ \zeta_2 = \frac{1}{h}\int_{-h/2}^{h/2} l_x^2\, dt \\ \zeta_3 = \frac{1}{h}\int_{-h/2}^{h/2} l_x^3 l_y\, dt \\ \zeta_4 = \frac{1}{h}\int_{-h/2}^{h/2} l_x l_y\, dt \end{cases} \tag{22}$$

where t is the layup through-thickness coordinate and h is the total layup thickness. The homogenized stiffness tensor of the complete layup is now defined as:

$$Q^H = \begin{bmatrix} A & B \\ B^T & D \end{bmatrix} \tag{23}$$

where **A** is the axial stiffness matrix, ***B*** is the shear/ axial coupling matrix and ***D*** is the shear stiffness matrix. The matrices ***A*** and ***D*** are symmetric. The non-zero components of the three matrices is defined as follows:

Accepted for publication in Composite Structures, Vol. 200, 15 Sept. 2018, Pages 781-79
https://doi.org/10.1016/j.compstruct.2018.05.078

$$\begin{bmatrix} A_{11} \\ A_{12} \\ A_{13} \\ A_{22} \\ A_{23} \\ A_{33} \end{bmatrix} = \begin{bmatrix} \zeta_1 & \zeta_2 & 0 & 0 & 1 & 0 & 0 & 0 \\ -\zeta_1 + \zeta_2 & 0 & 0 & 0 & 0 & 1 & 0 & 0 \\ 0 & 0 & \zeta_2 & 0 & 0 & 0 & 1 & 0 \\ \zeta_1 - 2\zeta_2 + 1 & -\zeta_2 + 1 & 0 & 0 & 1 & 0 & 0 & 0 \\ 0 & 0 & -\zeta_2 & 1 & 0 & 0 & 0 & 0 \\ 0 & 0 & 0 & 0 & 0 & 0 & 0 & 1 \end{bmatrix} \begin{Bmatrix} U_1 \\ U_2 \\ U_3 \\ U_4 \\ U_5 \\ U_6 \\ U_7 \\ U_8 \end{Bmatrix} \tag{24}$$

$$\begin{bmatrix} B_{11} \\ B_{12} \\ B_{13} \end{bmatrix} = \begin{bmatrix} \zeta_3 & \frac{1}{2}\zeta_4 & 0 \\ -\zeta_3 + \zeta_4 & \frac{1}{2}\zeta_4 & 0 \\ 0 & 0 & \zeta_4 \end{bmatrix} \begin{Bmatrix} U_1 \\ U_2 \\ U_3 \end{Bmatrix} \tag{25}$$

$$\begin{bmatrix} D_{11} \\ D_{22} \\ D_{23} \\ D_{33} \end{bmatrix} = \begin{bmatrix} -\zeta_1 + \zeta_2 & 1 & 0 & 0 & 1 \\ 0 & 0 & 1 & 0 & \zeta_2 \\ 0 & 0 & 0 & 0 & \zeta_4 \\ 0 & 0 & 0 & 1 & -\zeta_2 \end{bmatrix} \begin{Bmatrix} U_1 \\ U_9 \\ U_{10} \\ U_{11} \\ U_{12} \end{Bmatrix} \tag{26}$$

In this form, the layup contribution to each term in the stiffness tensor can be identified. It is worth mentioning that the kinematic homogenization approach yields shear/axial coupling terms in the stiffness tensor which are $Q_{XXXY}, Q_{XXYZ}, Q_{YYXY}, Q_{YYYZ}, Q_{XYYZ}$. These terms are suitable for use directly with 3D solid elements. Also, the in-plane / out-of-plane coupling terms given here will not be captured by CLA based lamination parameters. A comparison between the results for four sample layups from periodic homogenization using the FE based models described in section 2 and the kinematic homogenization with 3D lamination parameters is given in Figure 5. For the case of a composite layup with no defects, the 3D lamination parameters match the response from periodic homogenization. Additionally, the lamination parameters can be solved analytically and thus have minimal computational expense. It is worth mentioning that the periodic homogenization using the FE/RVE approach calculates the full fourth order stiffness tensor. The zero stiffness terms from the 3D lamination parameters approach (Equation 23) were also calculated as zero in the FE/RVE approach for all cases.

3.2 Design Space Sampling

The 3D lamination parameters provide a quick and accurate approach to calculating the stiffness response of thick composites. However, this approach does not include the effect of internal defects and features.

Here, a surrogate model has been developed to modify the kinematic homogenization results to account for internal defects. An initial step for building a surrogate model is to define the feasible regions of the design space. Once the boundaries are defined the design space can be sampled to select a set of design points to be modelled explicitly. Based on the lamination parameters identified in the previous section $\{\zeta_1,\ldots,\zeta_4\}$, the design space for a thick composite is a 4-dimension hyperspace. Several approaches have been proposed in the literature to define the boundaries for a design space using CLA lamination parameters [38]. This paper follows the approach proposed by Hammer et al [27]. In this approach, the boundary defined in the lamination parameters hyperspace is projected onto four 3D spaces. In each of these spaces one of the lamination parameters is equal to zero. The domain boundary can then be applied to each of the 3D spaces separately. To populate the design space, a Monte Carlo algorithm is used to generate random composite layups and calculate the associated lamination parameters. Once the design space has been populated a convex hull can be used to identify the design space boundary in each of the 3D design spaces, following the approach proposed by Setoodeh [39].

Following from the boundary definition, a Full Factorial Design (FFD) is used to select sample points in the hyperspace (ζ). The results from FFD is a 4D mesh which is projected on each of the four 3D domains. Then using a 3D Delaunay triangulation of the boundary, the grid points are compared against the boundary projections. Grid point projections have to fall inside all four boundaries to be considered a feasible design point. The 4D mesh density can be used to control the number of models solved to sample the design space. In this work, 86 design points were identified inside the domain boundary using an FFD for 10 lamination parameters increments which were solved against 4 defect severity increments. Figure 6 shows the design space boundary projections and the sampled points. The Latin Hyper Cube (LHC) approach was initially considered for design space sampling since LHC can sample a design space with fewer points than the FFD approach used here. However, LHC under-samples the domain boundaries which introduced surrogate model errors for layups lying on the domain boundaries. In practice, composite designers tend to use standard ply orientations such as 0, 90, +/- 45; these ply angles lie on the design space boundaries. As a result, the surrogate model errors on the boundaries greatly reduce the overall accuracy. Consequently, an equidistant mesh was adopted, since in this approach the design space boundary can be sampled directly.

In the design space of lamination parameters, each design point is defined by a set of four lamination parameters. To build an FE model corresponding to these points, the layup has to be defined explicitly using ply orientations instead of lamination parameters. This is an inverse open-ended problem where the number of feasible solutions will change based on the number of plies in any given layup. In this paper, the number of plies for the test layups has been set to 32, to allow for the insertion of defects in the FE - RVE, as required. A nonlinear solver was used to find the layups that would satisfy the lamination parameters at each design point. The nonlinear solver uses a Levenberg-Marquardt algorithm to minimize a residual vector between the lamination parameters from a proposed layup and the design point. Figure 7 shows a flow chart for the design space sampling process.

A fifth design parameter can be added to represent the defect severity. Out-of-plane wrinkles have been selected to demonstrate the modelling approach. Four defect levels were applied at each of the design points, based on the wrinkle angle (0°, 5°, 8° and 11°). An FE-RVE model is built for each design point and for each defect level. The models were solved and submitted for computational homogenization, following the procedure defined in section 2. In total, 366 models were solved. These models are divided as 86 models for each defect severity. It is worth mentioning that in the sampling approach used in this work, the number of sampling points is not determined beforehand since the domain boundary is determined numerically by testing design points. Here, each design variable is sampled by 10 points and 4 defect severity levels. Using this approach, the 13 elastic constants forming the stiffness tensor for each case are identified. An RVE database combining the lamination parameters, defect severity and the corresponding elastic constants was compiled. This database will be used as basis for fitting the surrogate model in the subsequent sections. An example record from this database is shown in Figure 8.

3.3 Surrogate Modelling using Chaos Polynomial Expansion

In the previous section, the lamination parameters were shown to control the stiffness response of the defect-free composite. In this section, a surrogate model based on the 3D lamination parameters is used to correct the kinematic stiffness tensor to account for the presence of the fibre waviness caused by the wrinkle defect. This can be achieved by writing the total stiffness tensor of an RVE in terms of a kinematic stiffness tensor and a correction tensor:

$$Q^X = Q_K^X - \Delta(\zeta) \tag{27}$$

The stiffness correction term $\Delta(\zeta)$ can be predicted using a surrogate model to account for the difference between the response of a pristine and a defective RVE. Several types of surrogate models have been used in modelling of composite materials. In this work, Chaos Polynomial Expansion (CPE) was employed to model the design space response. This approach has been successfully used to quantify uncertainties resulting from internal defects in composite materials [40, 41] . Hermite functions coupled with a second order expansion were fitted to the responses database to form the surrogate models. The expansion and Hermite functions are given by Equation 28a and 28b. Equation 29 shows an example of applying the expansion to the stiffness term Q_{XXXX}.

$$\Delta(\zeta) = a_0 H_0 + \sum_{i_1=1}^{\infty} a_{i_1} H_1(\zeta_{i_1}) + \sum_{i_1=1}^{\infty} \sum_{i_2=1}^{i_1} a_{i_1 i_2} H_2(\zeta_{i_1}, \zeta_{i_2}) \tag{28a}$$

$$Hermite\ functions \begin{cases} H_0 = 1 \\ H_1 = \zeta \\ H_2 = \zeta^2 - 1 \end{cases} \tag{28b}$$

$$\Delta(\zeta)\, Q_{XXXX} = a_0 + a_1\zeta_1 + a_2\zeta_2 + a_3\omega + a_4(\zeta_1^2 - 1) + a_5\zeta_1\zeta_2 + a_6\zeta_1\omega + a_7(\zeta^2 - 1) + a_8\zeta_2\omega + a_9(\omega^2 - 1) \quad (29)$$

A non-linear regression fit algorithm using least square estimation approach was used to calculate the values of the expansion constants a_{ij} to fit the response from the database. In this work the MATLAB function *nlinfit* was applied to fit the regression constants for each of the 13 terms in the stiffness tensor independently. A separate surrogate model is fitted for each elastic constant. The models fitted here are dependent on the material invariants and consequently are only suitable for the material system used to build them. In this case, the material is IM7/8552 pre-preg. Invariant based approaches presented in the literature can potentially be used to develop a material system-independent approach in the future [42]. The relation between the elastic constants and the lamination parameters can be found by studying the ***A***, ***B***, and ***D*** matrices. Table 1 shows the relation between the lamination parameters and the elastic constants as well as the number of fitting constants for each model.

This surrogate model can be used to generate maps of the elastic constants of a composite material vs the 3D lamination parameters. Using these maps the designers can develop a deep understanding of the design space and the impact of possible defects. Structural properties can be tailored to have a specific response or tolerance to a specific level of defect. Figure 9 shows maps of the elastic constants Q_{XXXX} , Q_{XXYY}, Q_{XXZZ} and Q_{YYZZ}. The constants are contoured vs the lamination parameters ζ_1, ζ_2 and the defect severity ω. The response shows that the axial elastic constants and the associated coupling terms are dependent on the wrinkle angle. Q_{XXXX} is more affected by waviness when the layup is zero dominated. For layups with low Q_{XXXX} , the effect of wrinkle severity on stiffness is minimal. On the other hand, the in-plane / out-of-plane coupling terms Q_{XXZZ} and Q_{YYZZ} increase considerably as the waviness angle increases. This observation can be attributed to the fact that waviness causes little disruption to the fibres lying across the waviness primary direction (e.g. 90° plies, when the 0° plies are wrinkled). On the other hand, the orientation of the fibres acting parallel to the wrinkle direction changes considerably. Consequently, these fibres contribute to the stiffness in the through-thickness direction and contribute to the in-plane/ out-of-plane coupling. Figure 10 shows the variation of the axial / shear coupling terms (Q_{XXXY} and Q_{ZZXY}) from the B matrix vs the lamination parameters ζ_3 and ζ_4 . The effect from introducing the wrinkle is minimal and was not included for these constants. The maps show the possibility of controlling these coupling terms and consequently tailoring structures for specific applications such as morphing structures. Figure 11 shows the effect of defect severity on the axial stiffness of a number of composite layups. This confirms the observation mentioned earlier that layups with higher axial stiffness are impacted by the presence of a wrinkle.

Accepted for publication in Composite Structures, Vol. 200, 15 Sept. 2018, Pages 781-79
https://doi.org/10.1016/j.compstruct.2018.05.078

4- Application to Macro-scale Models

4.1 Concurrent multiscale modelling

The surrogate model developed in the previous section can be used as a constitutive law linking the macro stresses and strains. In this work, the surrogate model was implemented as a UMAT subroutine in ABAQUS/standard. The macro/ meso link is implemented using a concurrent multiscale modelling approach. In Finite Element Squared (FE2) models, each integration point is assigned an RVE that represents the material's underlying meso-structure [43, 44] with the macro model and RVE models being solved simultaneously. The macro-strain is applied to the RVE model, then equivalent material properties are fed-back to the macro-scale. Overall FE2, is an effective multi-scale modelling approach that can handle both linear and non-linear problems. However, due to the need to run a macro-model and various RVE models concurrently, it is associated with a high computational expense. In the current work, the feedback loop is modified to use the surrogate model instead of a full FE-RVE. The first step of the proposed approach is the mapping of the composite layup onto a macro-scale mesh. A virtual RVE is constructed around every integration point in the macro-scale mesh. The virtual RVE size is set equal to the macro-element characteristic length. This virtual RVE is compared against the layup definition and the plies lying inside this RVE are identified. Next, the lamination parameters for the plies inside the RVE are calculated and assigned to the integration point. Figure 12a shows a schematic for a virtual RVE construction. It is worth mentioning that for fully integrated elements a virtual RVE will expand beyond the macro-element boundaries and will overlap with RVEs from adjacent integration points.

In conventional FE modelling, the mesh is selected to follow the structure geometric features. For instance, in a high-fidelity composite model, the elements size will be selected to match the ply thickness and follow the ply paths. However, for macro-scale modelling, the orientations of the elements may not be related to the internal material architecture or the underlying composite layup. To link the macro mesh and the underlying virtual RVE, three different axes are needed. These axes are the RVE axis, the Macro-element axis, and the global axis. Both the surrogate model and the kinematic homogenization predict the stiffness tensor in the RVE axis. In these models, the composite layup is oriented so that the 0° fibre direction is aligned along the RVE X-axis. There is no guarantee a macro-element axis is always aligned with the RVE X-axis. Thus, a rotation is applied to the stiffness tensor calculated from the surrogate model, based on comparing the macro-element axis to the layup orientation at any given location. This is especially important for composites with tapers and ply drops. Figure 12b shows the relation between the element axis and the RVE axis. The wrinkle severity can now be quantified by measuring the out-of-plane angle between any ply axis and the RVE X-axis. The maximum waviness angle seen in any given virtual RVE is taken as the defect severity and is assigned to the macro-element integration point. Once the mapping is complete, every macro-scale integration point is defined by a full set of lamination parameters and wrinkle or defect severity. The lamination parameters and defect severity are assigned to each integration point

before starting the macro-scale simulation. The defect severity is calculated by scaling the defect level (the wrinkle angle in this case) by the fraction of the RVE volume affected by the defect following Equation (30):

$$\omega_{RVE} = \frac{V_{Defect}}{V_{RVE}} \omega_{Defect} \tag{30}$$

where ω_{RVE} is the effective macro-scale defect severity, V_{Defect} is the volume of the RVE portion affected by the wrinkle, V_{RVE} is the total RVE volume and ω_{Defect} is the defect level (for the wrinkle type defect this is the wrinkle angle). In the current work, the model preparation steps are carried out automatically as part of the pre-processing phase. The lamination parameters and defect severity are added to the ABAQUS models as initial conditions for the solution dependent state variables using the *INITIALCONDITIONS keyword. During the macro-scale simulation, a UMAT subroutine reads the state variables and then uses the surrogate model to calculate the stiffness tensor for each integration point. The meso-scale ply orientations and the wrinkle angles are user inputs for the structure being modelled.

4.2 Numerical Examples

In this section, a set of numerical examples is presented to demonstrate the multiscale approach capabilities. The multiscale models are compared against equivalent high fidelity ply-by-ply models of the same structures. The purpose is to evaluate the ability of the proposed approach to predict the stiffness and average stress in a composite structure with waviness and ply drops. In the first model, a beam containing a waviness region and under tensile load is modelled using both approaches. Multiple models with different waviness severities ranging from 0° to 11° were solved under load control for both approaches. The meso-scale model was built as a ply-by-ply model using 64 linear Hexahedral elements through the thickness, representing each ply of the quasi-isotropic $[45/90/-45/0]_{8S}$ layup. Additionally, the waviness is modelled explicitly as a cosine function following Mukhopadhyay [9]. On the other hand, the macro model is defined by 6 reduced integration Hexahedral elements through the thickness. The displacement fields predicted by both models are shown in Figure 13, as well as the defect severity mapped over the macro-scale mesh. A comparison between the beam tip displacement from the macro and high fidelity models vs the waviness severity is shown in Figure 14. The tip displacement and the displacement fields are in good agreement. Figure 15 shows a comparison between the pristine cantilever beam natural frequencies from both the meso and multiscale models. The wrinkle defect was found to have minimal impact on the beam natural frequencies hence was not included in the comparison presented in Figure 15.

Another example is a thick twisted plate, fixed in a cantilever position and modelled under a body load along its length (representative of centrifugal loading). The twisted structure provides a more complex

geometry and a more complex stress state compared to the previous example. An unbalanced layup $(0/90/45/0)_{2S}$ was used to introduce a coupled response and evaluate if the multi-scale model can capture complex material response. The multi-scale model was built using 2 second order hexahedral elements through the thickness as opposed to 16 in the case of the high-fidelity model. No defect was introduced in this case. The displacement field from both the multi-scale and meso models are shown in Figure 16. A comparison of the stress fields averaged through the plate thickness is shown in Figure 17. The different average stress components can be seen to be matching between both the multiscale and high-fidelity models including the unsymmetrical response resulting from the chosen layup.

Finally, a model of a tapered composite structure with ply drops and localised waviness was modelled, as shown in Figure 18. The model is of a laminate made from Hexcel's IM7/8552 prepreg material with thickness of 80 mm at the thick end and 20 mm at the narrow end. The structure uses a $(0/\pm45)$ layup and is described in detail in the work by Gan et al [45]. This specimen is a generic feature that commonly appears in thick composite structures where a change in component thickness is required. This tapered specimen is a challenging benchmark problem combining complex geometry with ply drops and induced wrinkles. To achieve the required change in thickness, multiple ply drops are introduced along the length of the structure. It has been shown that ply drops can cause localized waviness around ply drop locations. These defects were included explicitly in a high-fidelity model of the specimen and are visible in Figure 18. The specimen is held in a socket, which is represented in the model by a rigid contact surface. Loading is via a prescribed displacement, applied at the narrow end. Only the upper half of the structure is modelled, with a symmetry boundary condition applied on the x-z plane. A single element across the width in the z direction is modelled under generalized plane strain boundary conditions. Two macro scale meshes of the same model with different levels of refinement have been built and mapped to the composites layup. Figure 19 shows a cut section of the macro model showing the element material axis assignment. The angle between the element material axis and the underlying RVE axis, as described in section 4.1, was included as a field variable and fed to the ABAQUS subroutine used with the model. Figure 19 also shows two different macro-scale meshes, High Density (HD) and Low Density (LD). Figure 20 shows a contour plot of the lamination parameter ζ_1 over the macro-scale mesh. The waviness severity is calculated for each virtual RVE and assigned to the associated integration point. Figure 21 shows a contour of the waviness severity over the macro-scale mesh. The model was solved in ABAQUS/explicit to allow for the inclusion of the contact boundary conditions. Additionally, the non-linear geometry option is used to allow the material axis to follow the element deformation. Consequently, the macro-scale stiffness tensor will always be aligned with the layup, even as the mesh deforms during the simulation. Figure 22 shows a plot of the total reaction force at the narrow end for both macro models (HD and LD) vs the high-fidelity model. The proposed multiscale approach shows good correlation with the high-fidelity model for both mesh densities. Additionally, the change in macro mesh size had little impact on the model response. Moreover, the response from a standard homogenisation approach with constant orthotropic properties over the whole model is also shown in Figure 22. The standard homogenization overestimates the component stiffness when compared to the high fidelity and multi-scale approaches. This is expected since traditional homogenisation does not include the effect of ply drops / waviness and does not represent the layup change

faithfully. Figure 23 shows the through thickness stress distribution over the macro (HD mesh) and meso models. The multiscale model can be seen to capture the general stress distribution across the structure. Regions with complex stress state such as the contact region and the taper regions show the same trend as the meso-models. The regions with ply drops and waviness show lower stresses compared to the pristine regions which was captured by both models.

5 – Discussion and Conclusions

In this paper, a novel multiscale modelling approach for thick composite structures with internal defects and features is developed. The proposed approach employs a surrogate model to include the meso-scale defects and features into a macro-scale simulation. One of the main challenges in multiscale of composites is the ability to include the meso-scale defects and features in a macro-scale model. In this work, a set of FE-RVE models were used to sample the design space and investigate the effect of defect severity on the composite behaviour. The RVE responses were then homogenized to calculate the effective response of those RVE models and convert their response in an average stress/strain relation. The average stress/ strain relation can be included as a 3D orthotropic material in the macro-scale model.

Since the composites response is dependent on the layup and the internal features, an RVE model for each layup / meso-scale feature has to be solved beforehand to calculate its equivalent response. In a complex structure, this will require numerous RVE models to be solved and homogenised. In this paper, the response from a discrete set of RVE models has been expanded using surrogate models to represent the complete design space. This required creating a link between the meso and macro-scales using the layup information. Normally, this is done using a set of lamination parameters derived from CLA. These lamination parameters however assume plate kinematics and are not suitable for thick structures. Here, a set of 3D lamination parameters have been developed to link the FE-RVE responses to the surrogate model.

A number of surrogate models have been tested to represent the defect severity on the macro-scale. CPE, which have been widely used in surrogate models for composite materials, was found to be the most suitable approach. Besides CPE, fitting a 3rd order polynomial, Artificial Neural Networks (ANN) and Response Surface Methodology (RSM) were tested. Figure 24 shows a comparison of the R^2 fit for each of the surrogate models tested for the first row of the stiffness tensor. For this study, an R^2 of 0.9 was selected as a threshold for a successful surrogate model. Only CPE and ANN cross this threshold. The ANN has been trained using 70% of the sampling points, 15% for validation and 15% for testing. A network with single hidden layer with 10 neurons was used for each elastic constant. ANN showed better fit overall for the test data than CPE. However, when the ANN was integrated in the concurrent multiscale model it showed poor robustness. Essentially, the ANN surrogate model generated large errors for cases that were not included in the training of the neural network, which is a common problem with this type of surrogate models. In this case, the errors from the ANN resulted in an inconsistent stiffness tensor leading the macro-scale simulation to crash. Consequently, CPE was selected as a good balance between accuracy and robustness. The framework presented here is suitable for integration with a variety of surrogate modelling approaches.

However, reviewing and assessing all possible surrogate modelling options was beyond the scope of this work.

The proposed approach was compared against high fidelity models for multiple cases. The multi-scale approach can predict the stiffness, natural frequencies, and average stresses with good accuracy. Additionally, the 3D lamination parameters include the complete through-thickness and coupling terms, thus allowing for the more complex 3D effects of defects / features to be included in the macro-scale simulation. The proposed approach has been shown to be an effective tool for modelling complex composite structures and understanding the effect of defects and features. The model maintains the average stresses and strains between the macro and meso-scales, while considering the heterogeneities resulting from the material internal architecture.

The proposed framework is generic and can be applied to different types of defects or features. In this paper, wrinkle defects are presented as an example. However, other types of defects can be introduced to the meso-scale RVE models. Figure 25 shows an example of other types of meso-scale defects or features. The figure shows the stress distribution from a quasi-isotropic layup with two cut plies at the centre of the RVE. The cuts have been introduced to the middle plies by changing the elements at the RVE centre to have matrix properties instead of ply properties. This discontinuous ply feature can be combined with other types of defects to develop a more complex RVE as shown in Figure 25c which combines the cut ply with a wrinkle. However, it is worth mentioning that the surrogate model used here was specifically built for wrinkle type defects. Introducing more complex defects might require more sampling points to capture the change in the mechanical response of the composite.

Acknowledgement

The authors wish to acknowledge the support Rolls-Royce plc through the Composites University Technology Centre (UTC) of the University of Bristol. The author's also acknowledge helpful discussions with Prof. Paul Weaver at the University of Bristol on the use of Lamination Parameters.

9 - References

[1] Stodieck, O., Cooper, J. E., Weaver, P. M. and Kealy, P. (2013) Improved aeroelastic tailoring using tow-steered composites. *Composite Structures*. **106** 703-715.
[2] Eastep, F., Tischler, V., Venkayya, V. and Khot, N. (1999) Aeroelastic tailoring of composite structures. *Journal of Aircraft*. **36**(6) 1041-1047.
[3] Lopes, C. S., Gürdal, Z. and Camanho, P. (2010) Tailoring for strength of composite steered-fibre panels with cutouts. *Composites Part A: Applied Science and Manufacturing*. **41**(12) 1760-1767.
[4] Haftka, R. T. and TARNES, J. H. (1988) Stiffness tailoring for improved compressive strength of composite plates with holes. *AIAA journal*. **26**(1) 72-77.
[5] Wisnom, M. R., Dixon, R. and Hill, G. (1996) Delamination in asymmetrically tapered composites loaded in tension. *Composite structures*. **35**(3) 309-322.

[6] Li, X., Hallett, S. R. and Wisnom, M. R. (2015) Modelling the effect of gaps and overlaps in automated fibre placement (AFP)-manufactured laminates. *Science and Engineering of Composite Materials*. **22**(2) 115-129.
[7] Falcó, O., Lopes, C., Naya, F., Sket, F., Maimí, P. and Mayugo, J. (2017) Modelling and simulation of tow-drop effects arising from the manufacturing of steered-fibre composites. *Composites Part A: Applied Science and Manufacturing*. **93** 59-71.
[8] Mukhopadhyay, S., Jones, M. I. and Hallett, S. R. (2015) Compressive failure of laminates containing an embedded wrinkle; experimental and numerical study. *Composites Part A: Applied Science and Manufacturing*. **73** 132-142.
[9] Mukhopadhyay, S., Jones, M. I. and Hallett, S. R. (2015) Tensile failure of laminates containing an embedded wrinkle; numerical and experimental study. *Composites Part A: Applied Science and Manufacturing*. **77** 219-228.
[10] Kerfriden, P., Allix, O. and Gosselet, P. (2009) A three-scale domain decomposition method for the 3D analysis of debonding in laminates. *Computational Mechanics*. **44**(3) 343-362.
[11] Kanouté, P., Boso, D., Chaboche, J. and Schrefler, B. (2009) Multiscale methods for composites: a review. *Archives of Computational Methods in Engineering*. **16**(1) 31-75.
[12] Hou, T. Y. and Wu, X.-H. (1997) A multiscale finite element method for elliptic problems in composite materials and porous media. *Journal of computational physics*. **134**(1) 169-189.
[13] Fukunag, H. and Vanderplaats, G. N. (1991) Stiffness optimization of orthotropic laminated composites using lamination parameters. *AIAA journal*. **29**(4) 641-646.
[14] Fukunaga, H. and Sekine, H. (1992) Stiffness design method of symmetric laminates using lamination parameters. *AIAA journal*. **30**(11) 2791-2793.
[15] Miki, M. and Sugiyamat, Y. (1993) Optimum design of laminated composite plates using lamination parameters. *AIAA journal*. **31**(5) 921-922.
[16] IJsselmuiden, S. T., Abdalla, M. M. and Gürdal, Z. (2010) Optimization of variable-stiffness panels for maximum buckling load using lamination parameters. *AIAA journal*. **48**(1) 134-143.
[17] Liu, B., Haftka, R. and Trompette, P. (2004) Maximization of buckling loads of composite panels using flexural lamination parameters. *Structural and Multidisciplinary Optimization*. **26**(1-2) 28-36.
[18] Fukunaga, H., Sekine, H., Sato, M. and Iino, A. (1995) Buckling design of symmetrically laminated plates using lamination parameters. *Computers & structures*. **57**(4) 643-649.
[19] Diaconu, C. G., Sato, M. and Sekine, H. (2002) Buckling characteristics and layup optimization of long laminated composite cylindrical shells subjected to combined loads using lamination parameters. *Composite Structures*. **58**(4) 423-433.
[20] Scarth, C., Cooper, J. E., Weaver, P. M. and Silva, G. H. (2014) Uncertainty quantification of aeroelastic stability of composite plate wings using lamination parameters. *Composite Structures*. **116** 84-93.
[21] Kameyama, M. and Fukunaga, H. (2007) Optimum design of composite plate wings for aeroelastic characteristics using lamination parameters. *Computers & structures*. **85**(3) 213-224.
[22] Thuwis, G. A., De Breuker, R., Abdalla, M. M. and Gürdal, Z. (2010) Aeroelastic tailoring using lamination parameters. *Structural and Multidisciplinary Optimization*. **41**(4) 637-646.
[23] Blom, A. W., Stickler, P. B. and Gürdal, Z. (2010) Optimization of a composite cylinder under bending by tailoring stiffness properties in circumferential direction. *Composites Part B: Engineering*. **41**(2) 157-165.
[24] Setoodeh, S., Abdalla, M. M. and Gürdal, Z. (2006) Design of variable–stiffness laminates using lamination parameters. *Composites Part B: Engineering*. **37**(4) 301-309.
[25] Khani, A., IJsselmuiden, S., Abdalla, M. and Gürdal, Z. (2011) Design of variable stiffness panels for maximum strength using lamination parameters. *Composites Part B: Engineering*. **42**(3) 546-552.

[26] Abdalla, M. M., Setoodeh, S. and Gürdal, Z. (2007) Design of variable stiffness composite panels for maximum fundamental frequency using lamination parameters. *Composite structures*. **81**(2) 283-291.
[27] Hammer, V. B., Bendsøe, M., Lipton, R. and Pedersen, P. (1997) Parametrization in laminate design for optimal compliance. *International Journal of Solids and Structures*. **34**(4) 415-434.
[28] De Carvalho, N., Pinho, S. and Robinson, P. (2011) Reducing the domain in the mechanical analysis of periodic structures, with application to woven composites. *Composites Science and Technology*. **71**(7) 969-979.
[29] Xia, Z., Zhou, C., Yong, Q. and Wang, X. (2006) On selection of repeated unit cell model and application of unified periodic boundary conditions in micro-mechanical analysis of composites. *International Journal of Solids and Structures*. **43**(2) 266-278.
[30] Jansson, S. (1992) Homogenized nonlinear constitutive properties and local stress concentrations for composites with periodic internal structure. *International journal of solids and structures*. **29**(17) 2181-2200.
[31] Michel, J., Moulinec, H. and Suquet, P. (1999) Effective properties of composite materials with periodic microstructure: a computational approach. *Computer methods in applied mechanics and engineering*. **172**(1) 109-143.
[32] Miehe, C., Schröder, J. and Becker, M. (2002) Computational homogenization analysis in finite elasticity: material and structural instabilities on the micro-and macro-scales of periodic composites and their interaction. *Computer Methods in Applied Mechanics and Engineering*. **191**(44) 4971-5005.
[33] Li, S. (2008) Boundary conditions for unit cells from periodic microstructures and their implications. *Composites Science and Technology*. **68**(9) 1962-1974.
[34] Tang, X. and Whitcomb, J. D. (2003) General techniques for exploiting periodicity and symmetries in micromechanics analysis of textile composites. *Journal of Composite Materials*. **37**(13) 1167-1189.
[35] Myers, R. H. and Montgomery, D. C. (1988) Response surface methodology. Taylor & Francis.
[36] Simpson, T. W., Mauery, T. M., Korte, J. J. and Mistree, F. (2001) Kriging models for global approximation in simulation-based multidisciplinary design optimization. *AIAA journal*. **39**(12) 2233-2241.
[37] Zhang, Z., Klein, P. and Friedrich, K. (2002) Dynamic mechanical properties of PTFE based short carbon fibre reinforced composites: experiment and artificial neural network prediction. *Composites Science and Technology*. **62**(7) 1001-1009.
[38] Bloomfield, M., Diaconu, C. and Weaver, P. (2008) On feasible regions of lamination parameters for lay-up optimization of laminated composites. *Proceedings of the Royal Society of London A: Mathematical, Physical and Engineering Sciences*. 465, 1123–1143. The Royal Society.
[39] Setoodeh, S., Abdalla, M. M. and Gürdal, Z. (2006) Approximate feasible regions for lamination parameters. *11th AIAA/ISSMO Multidisciplinary Analysis and Optimization Conference*. Portsmouth. vol. 2, pp. 814-822.
[40] Georgiou, G., Manan, A. and Cooper, J. (2012) Modeling composite wing aeroelastic behavior with uncertain damage severity and material properties. *Mechanical Systems and Signal Processing*. **32** 32-43.
[41] Xiu, D. and Karniadakis, G. E. (2002) The Wiener--Askey polynomial chaos for stochastic differential equations. *SIAM journal on scientific computing*. **24**(2) 619-644.
[42] Tsai, S. W. and Melo, J. D. D. (2014) An invariant-based theory of composites. *Composites Science and Technology*. **100**(Supplement C) 237-243.
[43] Feyel, F. and Chaboche, J.-L. (2000) FE 2 multiscale approach for modelling the elastoviscoplastic behaviour of long fibre SiC/Ti composite materials. *Computer methods in applied mechanics and engineering*. **183**(3) 309-330.

[44] Feyel, F. (2003) A multilevel finite element method (FE 2) to describe the response of highly non-linear structures using generalized continua. *Computer Methods in applied Mechanics and engineering*. **192**(28) 3233-3244.
[45] Gan, K. W., Allegri, G. and Hallett, S. R. (2016) A simplified layered beam approach for predicting ply drop delamination in thick composite laminates. *Materials & Design*. **108** 570-580.

Accepted for publication in Composite Structures, Vol. 200, 15 Sept. 2018, Pages 781-79
https://doi.org/10.1016/j.compstruct.2018.05.078

FIGURES

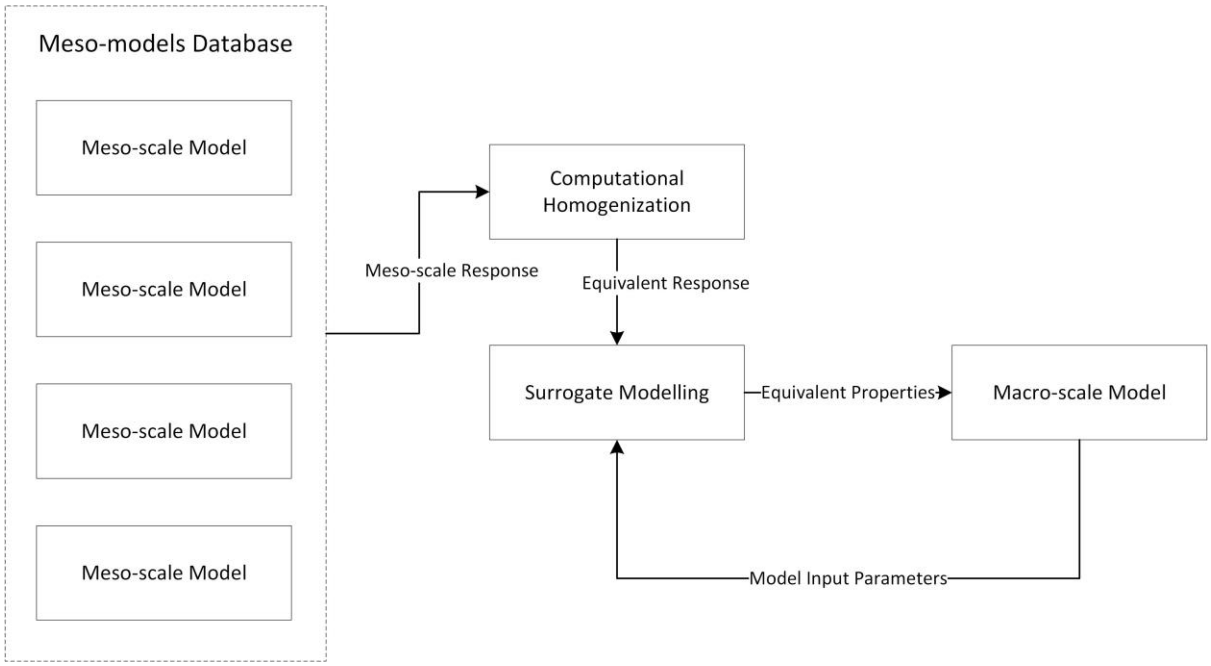

Figure 1. Surrogate multiscale modelling approach overview.

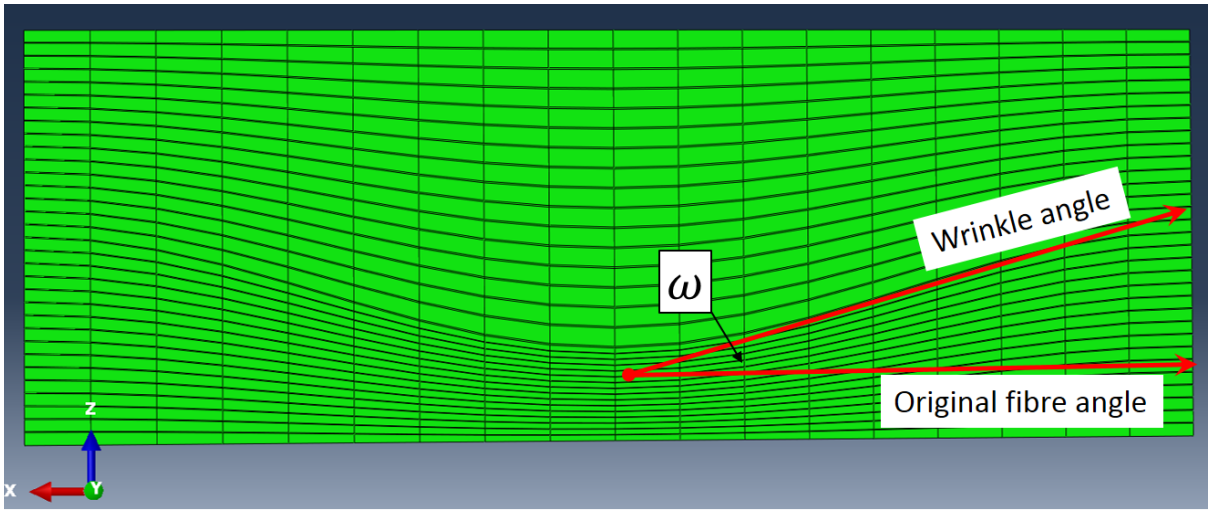

Figure 2. Wrinkle angle definition.

Accepted for publication in Composite Structures, Vol. 200, 15 Sept. 2018, Pages 781-79
https://doi.org/10.1016/j.compstruct.2018.05.078

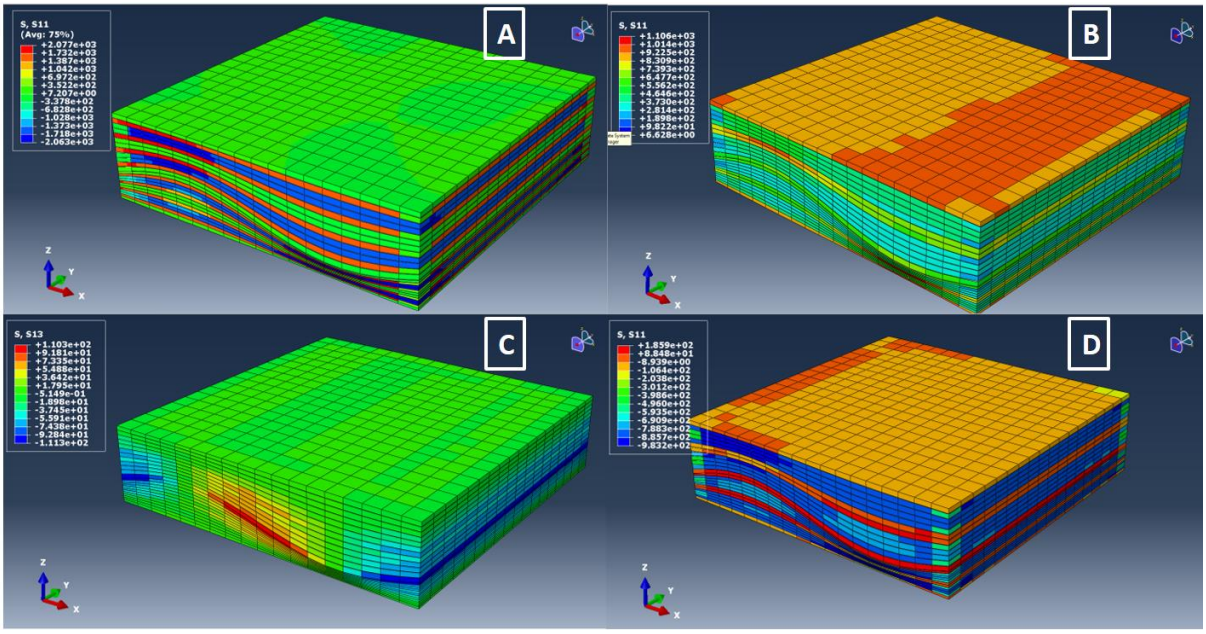

Figure 3. Typical unit cell models for a composite with QI layup containing a waviness defect, A) Fibre stresses under load in X direction, B) Fibre stresses under load in Y direction, C) Through thickness shear stresses under load in Z direction, D) Fibre stresses under shear load in X-Y plane.

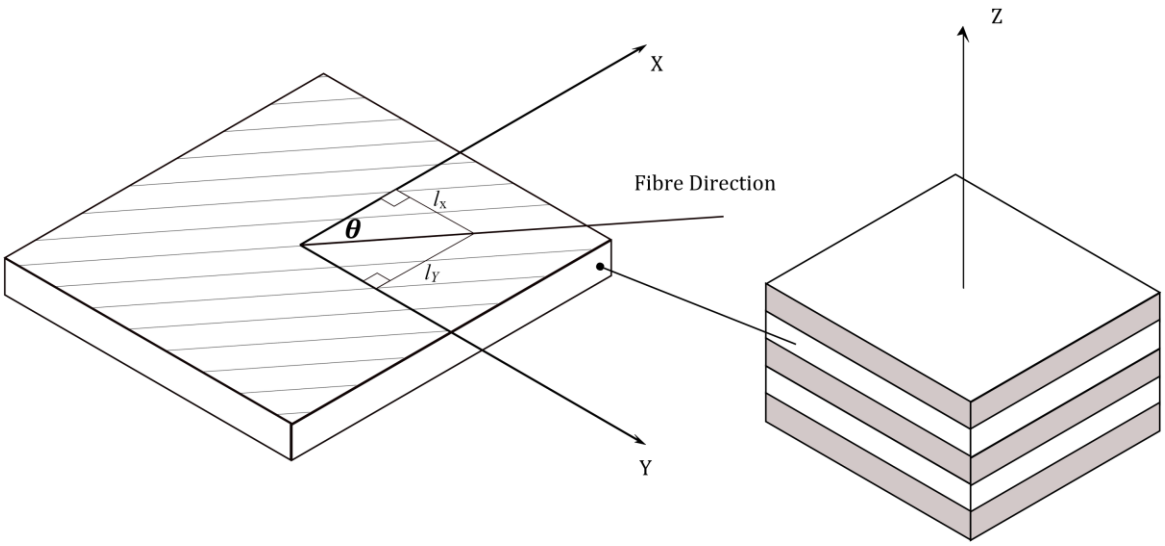

Figure 4. The relation between the ply angle and the direction cosines l_x and l_y.

Accepted for publication in Composite Structures, Vol. 200, 15 Sept. 2018, Pages 781-79
https://doi.org/10.1016/j.compstruct.2018.05.078

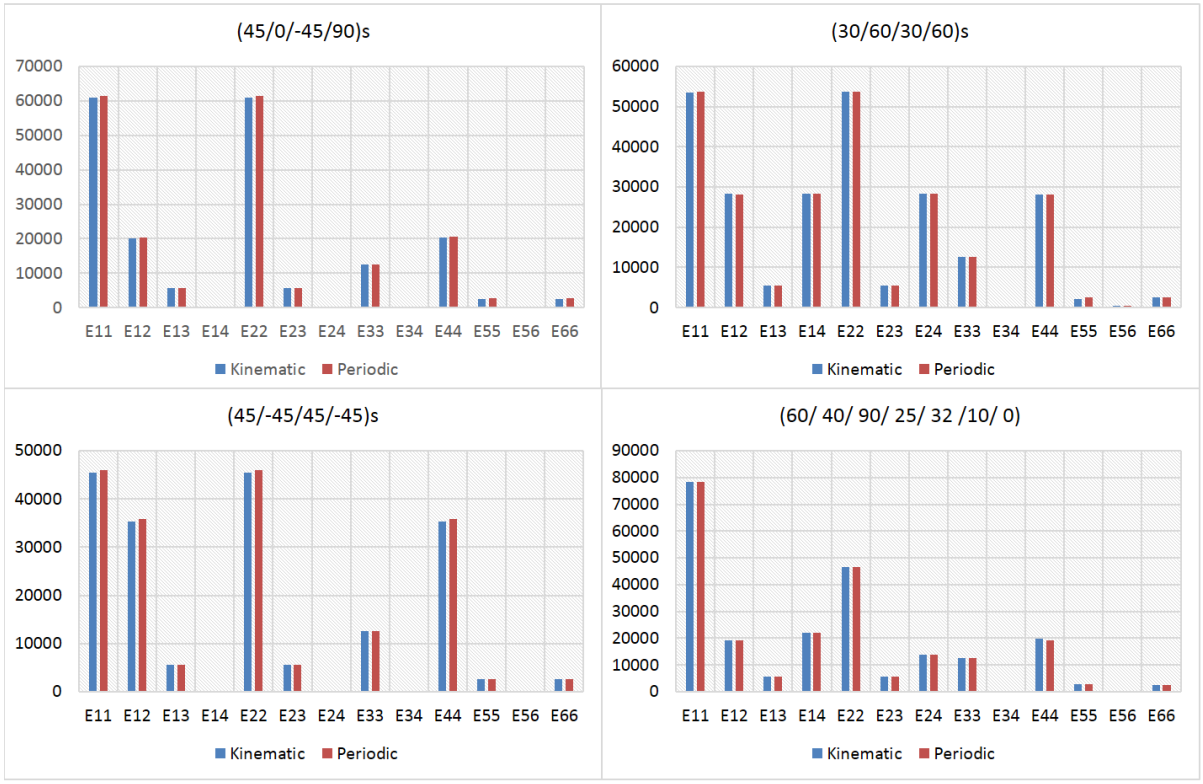

Figure 5. A comparison between stiffness (MPa) predictions from kinematic and periodic homogenization approaches for different layups with no defects.

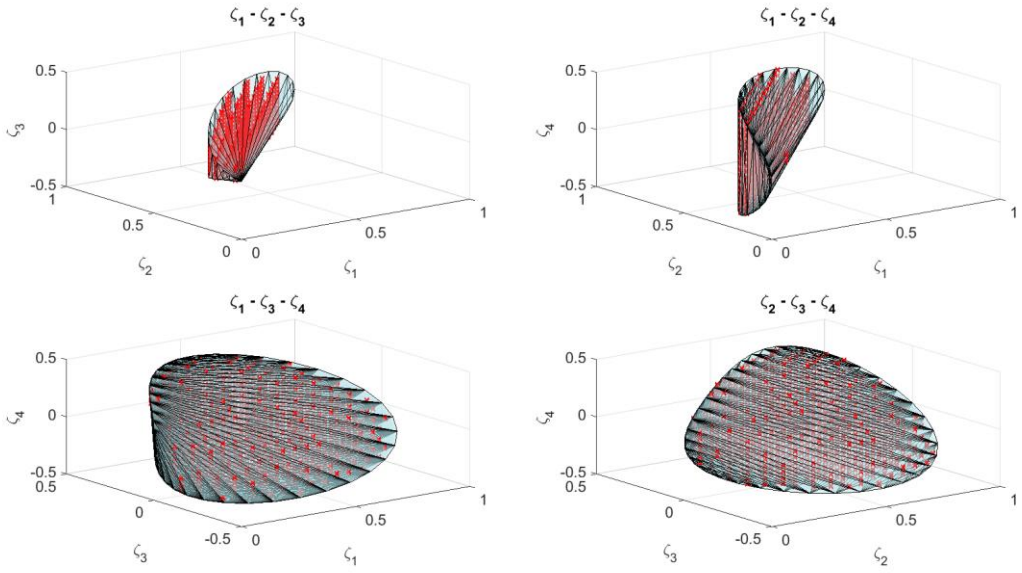

Figure 6. Design space boundaries and discretization. Feasible design points are shown as red crosses.

Accepted for publication in Composite Structures, Vol. 200, 15 Sept. 2018, Pages 781-79
https://doi.org/10.1016/j.compstruct.2018.05.078

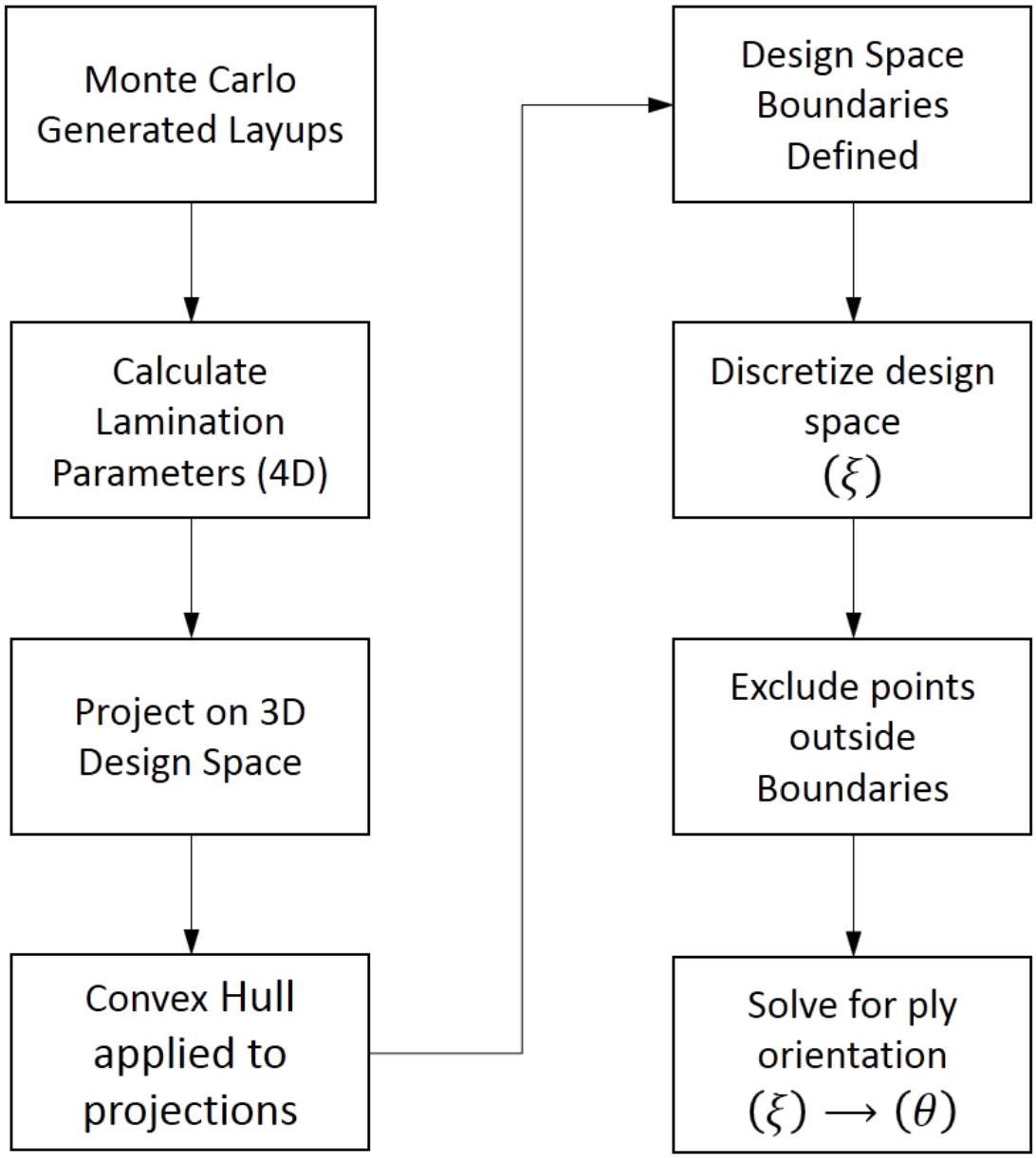

Figure 7. Flowchart of design space sampling.

ID	Lamination Parameters	Defect Severity	***A*** Matrix	***B*** Matrix	***D*** Matrix
i	$\xi_1, \ldots, \xi_4$	ω	$A_{11}, \ldots, A_{33}$	$B_{11}, \ldots, B_{13}$	$D_{11}, \ldots, D_{33}$

Figure 8. An example RVE database record.

Accepted for publication in Composite Structures, Vol. 200, 15 Sept. 2018, Pages 781-79
https://doi.org/10.1016/j.compstruct.2018.05.078

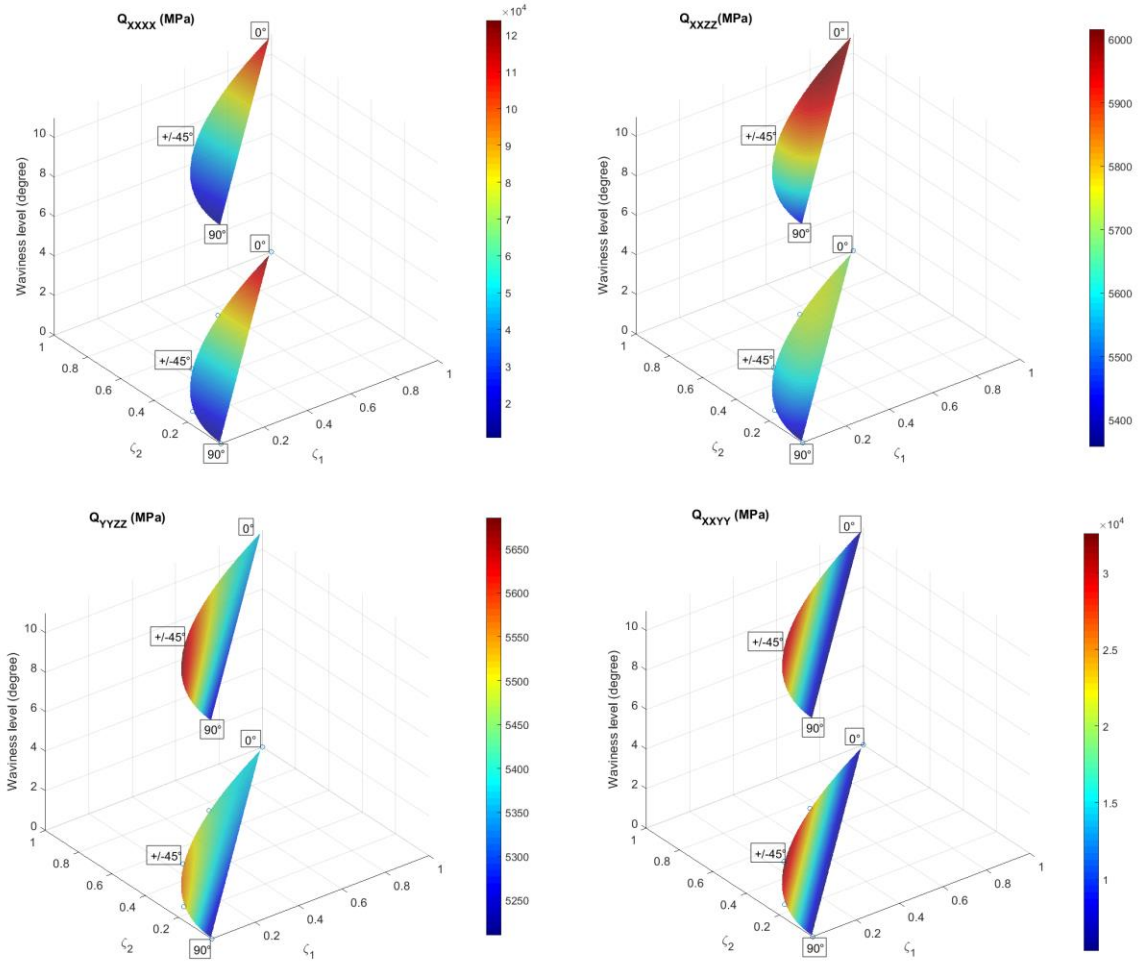

Figure 9 Stiffness tensor components vs lamination parameters and defect severity at 0° and 11°.

Accepted for publication in Composite Structures, Vol. 200, 15 Sept. 2018, Pages 781-79
https://doi.org/10.1016/j.compstruct.2018.05.078

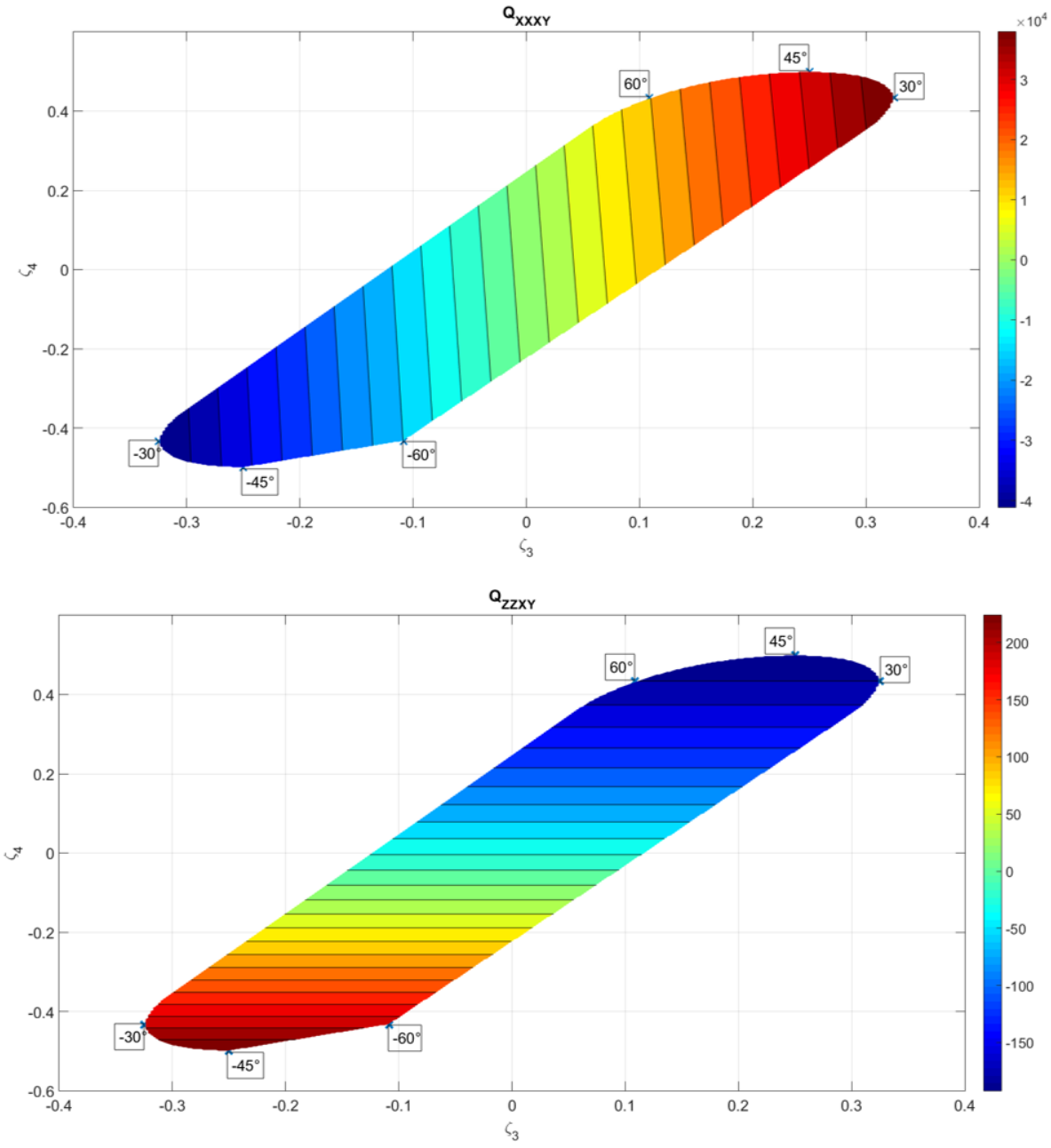

Figure 10. A contour map of Q_{XXXY} and Q_{ZZXY} over the design space.

Accepted for publication in Composite Structures, Vol. 200, 15 Sept. 2018, Pages 781-79
https://doi.org/10.1016/j.compstruct.2018.05.078

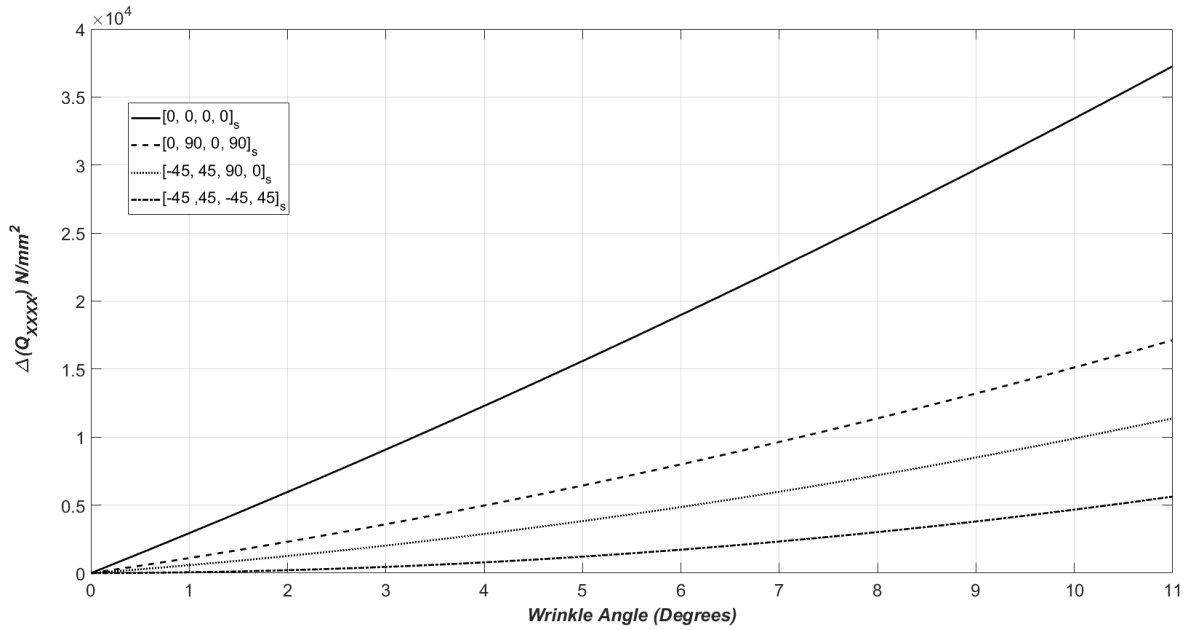

Figure 11. Axial stiffness of selected layup versus defect severity as predicted by the surrgoate model.

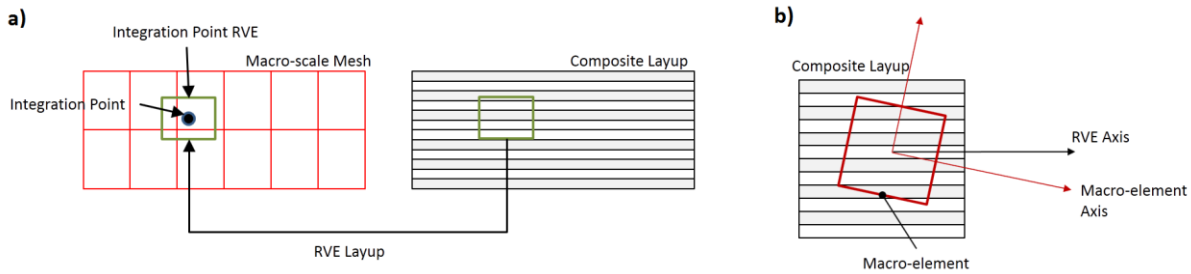

Figure 12. Construction of Integration Point RVE, a) Layup mapping and b) RVE axis and Macro-element axis definition.

Accepted for publication in Composite Structures, Vol. 200, 15 Sept. 2018, Pages 781-79
https://doi.org/10.1016/j.compstruct.2018.05.078

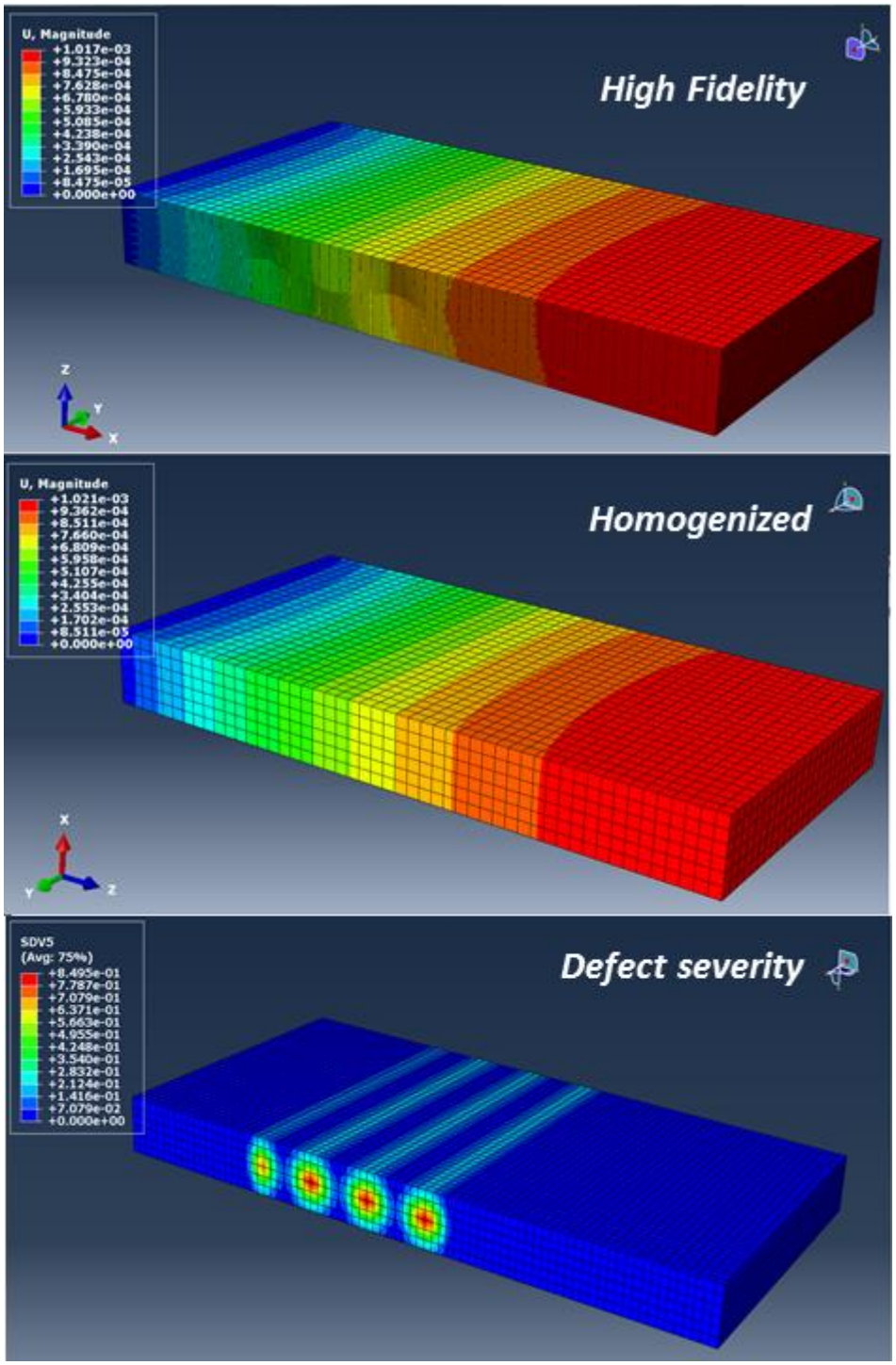

Figure 13. Displacement plots for a composite beam containing a 11 ° waviness under tensile loading.

Accepted for publication in Composite Structures, Vol. 200, 15 Sept. 2018, Pages 781-79
https://doi.org/10.1016/j.compstruct.2018.05.078

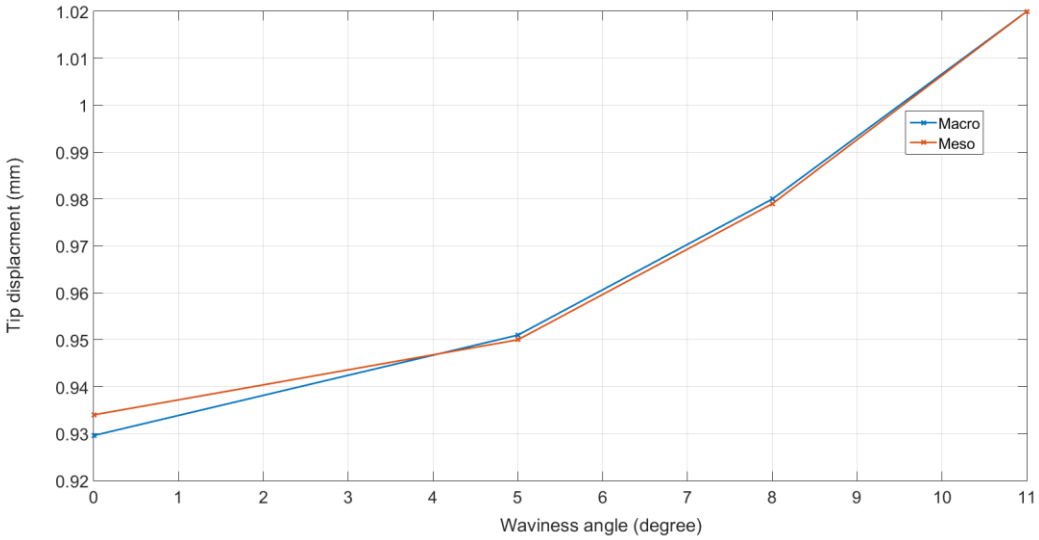

Figure 14. A comparison between the high fidelity and multiscale models responses.

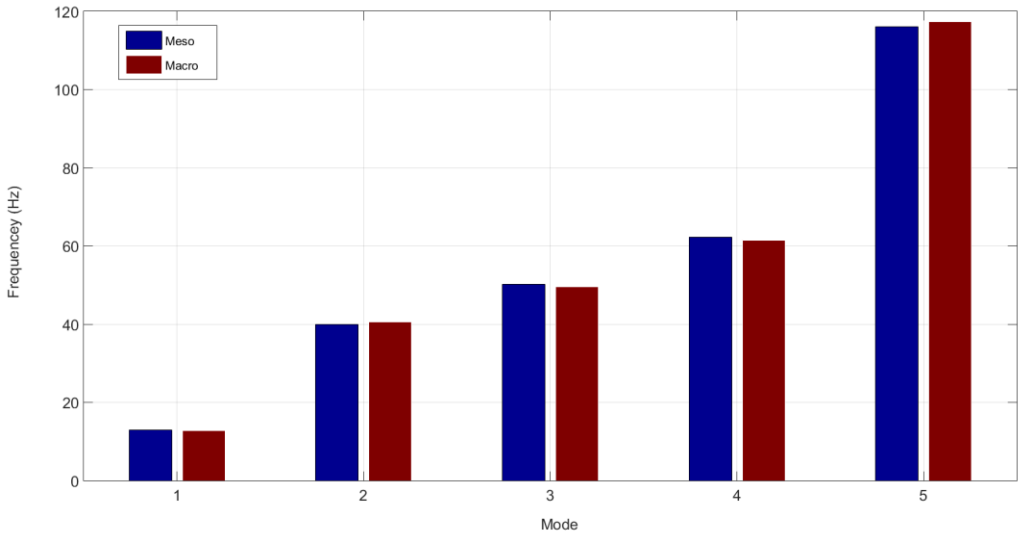

Figure 15. Mode frequency comparison between macro and meso models for a defect free cantilever beam.

Accepted for publication in Composite Structures, Vol. 200, 15 Sept. 2018, Pages 781-79
https://doi.org/10.1016/j.compstruct.2018.05.078

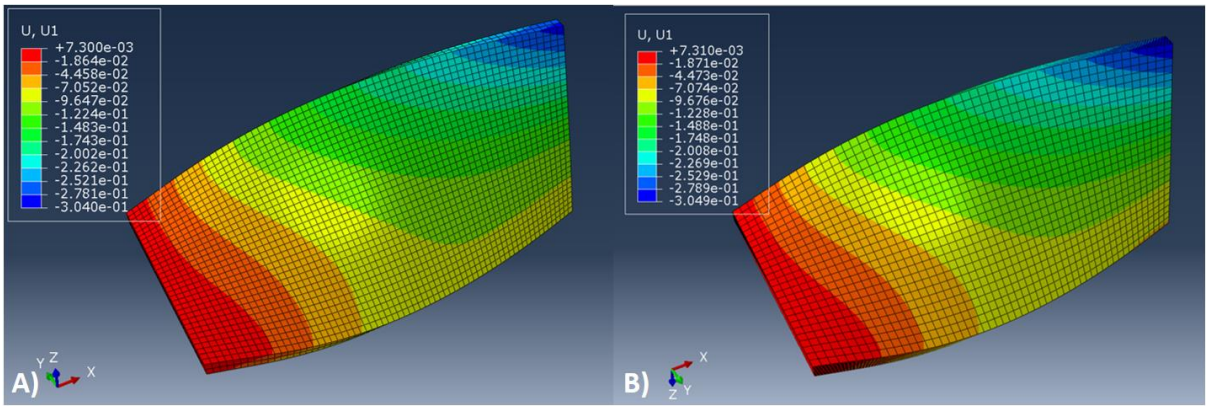

Figure 16. A comparison between the displacement from high fidelity and multi-scale models of a twisted plate: a) Multiscale; b) high fidelity.

Accepted for publication in Composite Structures, Vol. 200, 15 Sept. 2018, Pages 781-79
https://doi.org/10.1016/j.compstruct.2018.05.078

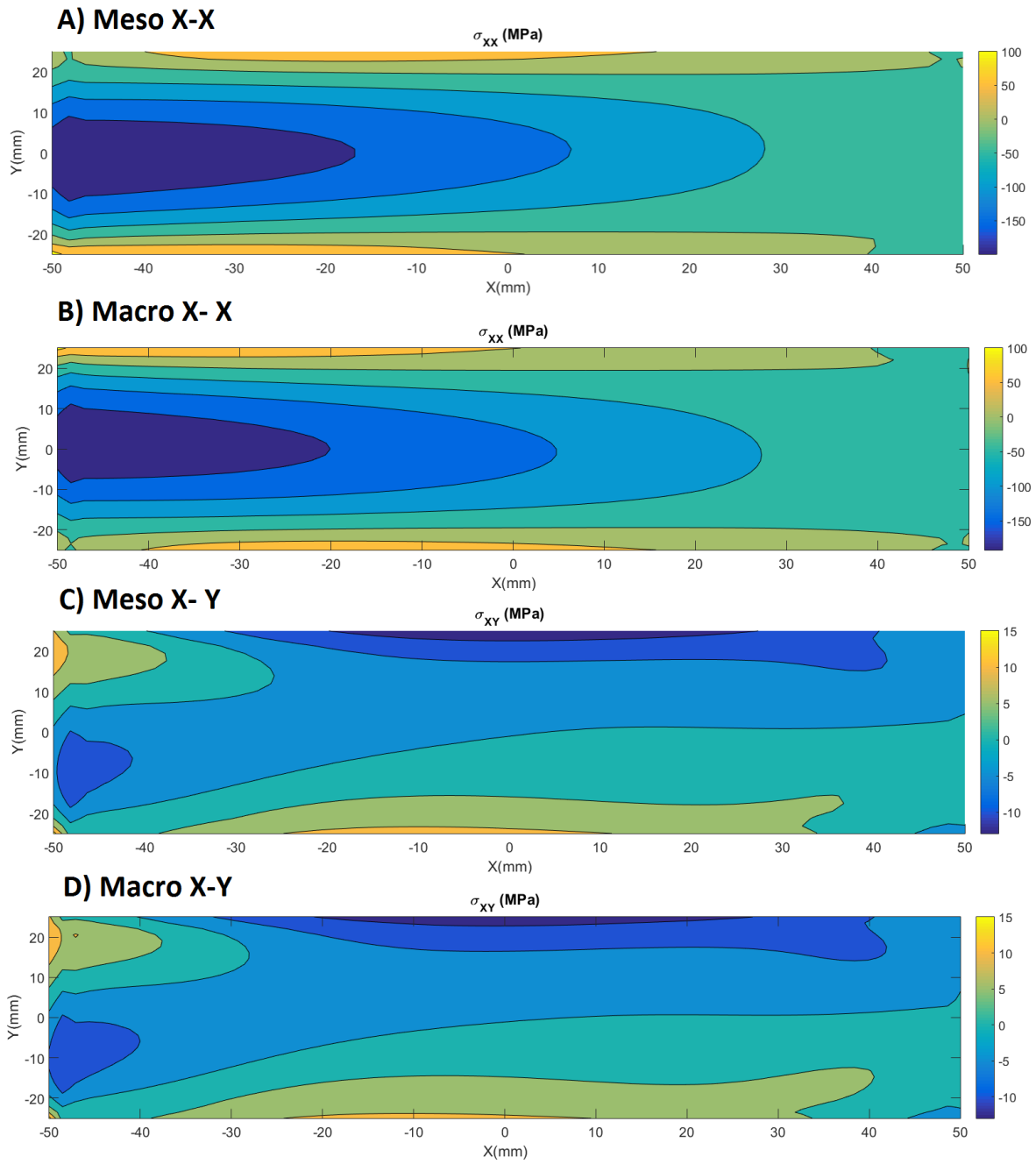

Figure 17. A comparison between the meso and macro model stresses for a twisted plate.

Accepted for publication in Composite Structures, Vol. 200, 15 Sept. 2018, Pages 781-79
https://doi.org/10.1016/j.compstruct.2018.05.078

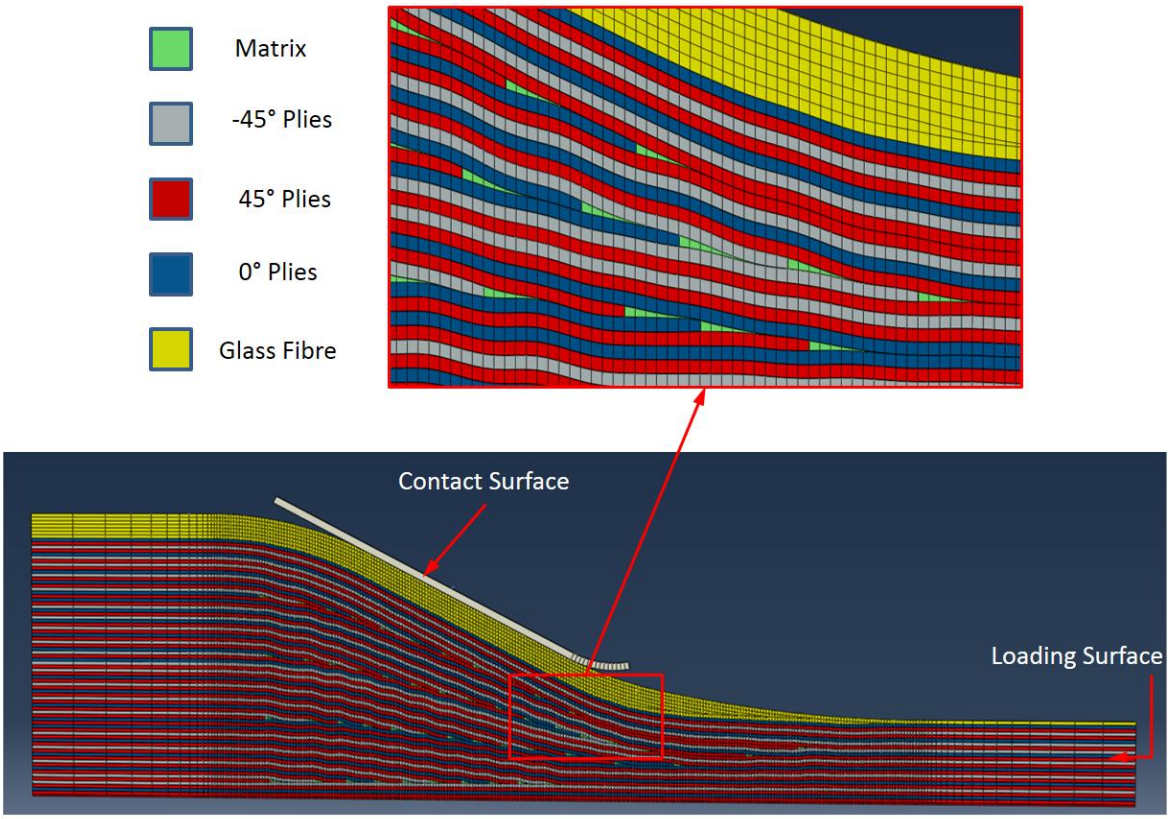

Figure 18 High fidelity model setup for a thick tapered lamina showing ply drops and the ply orientations.

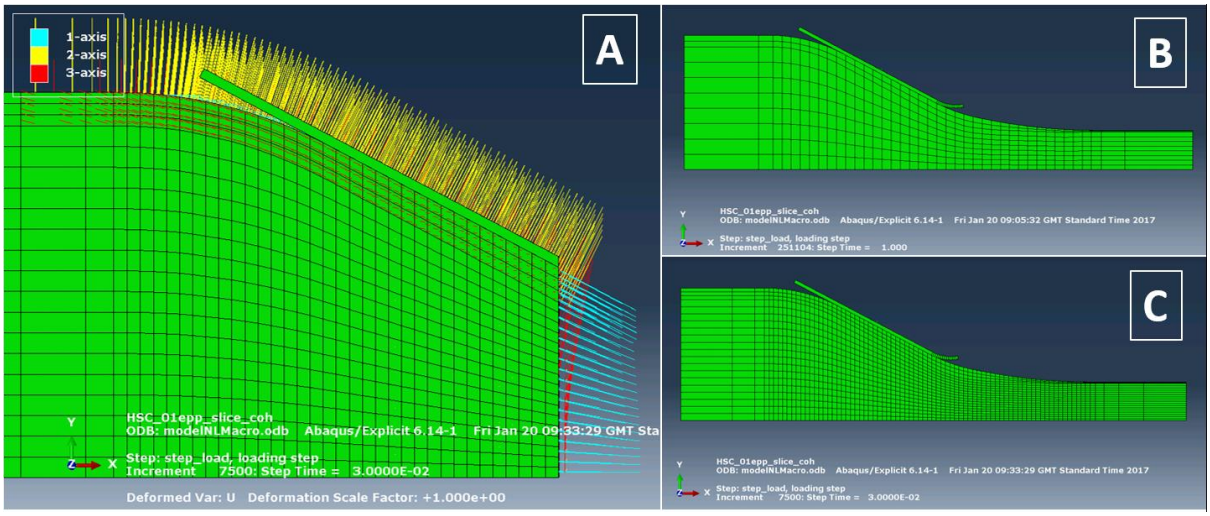

Figure19. Macro model setup for the tapered lamina: a) Cut section showing material axis assignment, b) Low density mesh, c) High density mesh.

Accepted for publication in Composite Structures, Vol. 200, 15 Sept. 2018, Pages 781-79
https://doi.org/10.1016/j.compstruct.2018.05.078

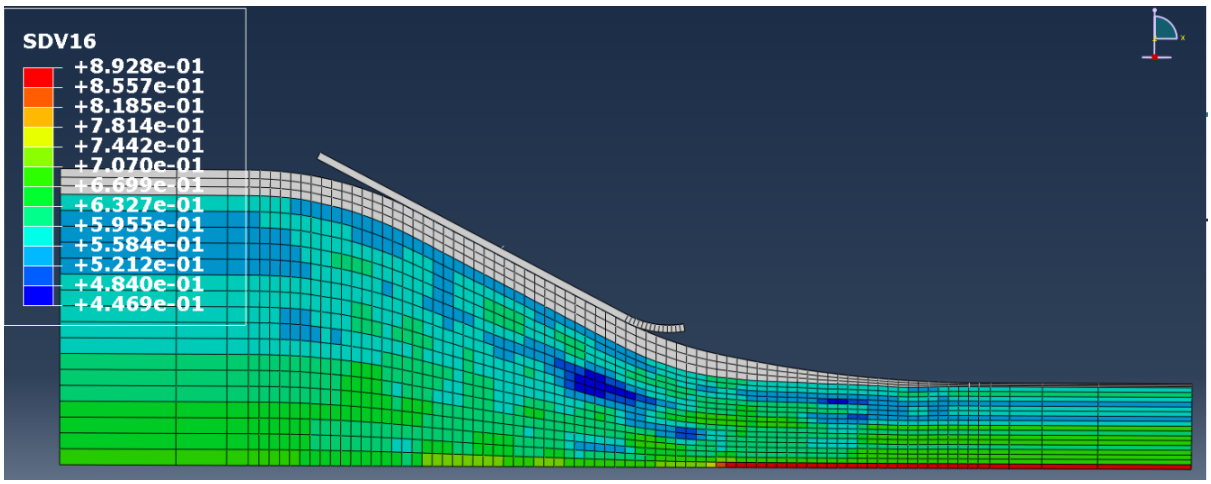

Figure 20. A contour plot of lamination parameters ζ_1 over the macro mesh.

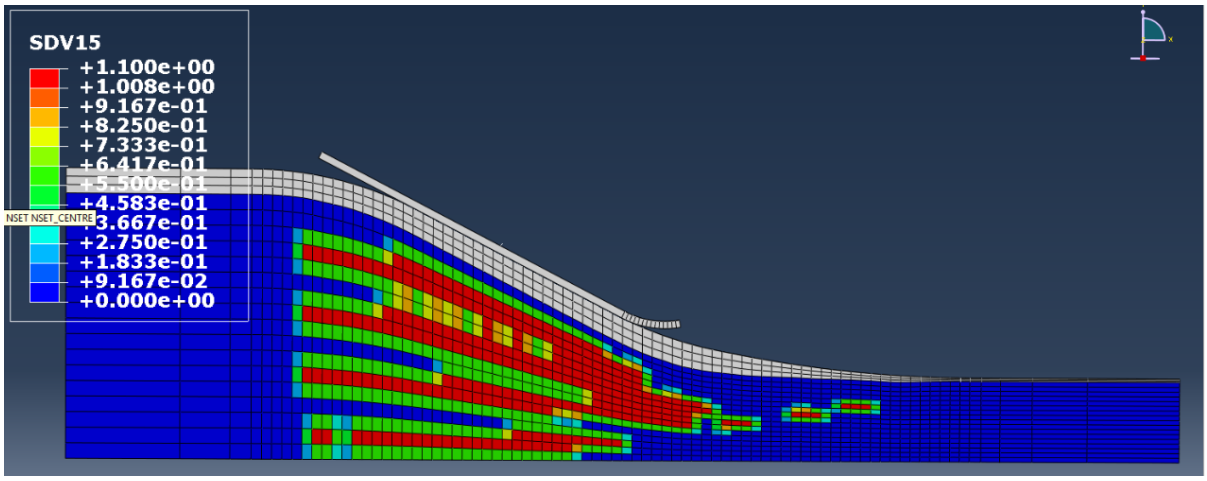

Figure 21 A contour plot of waviness severity over the macro mesh.

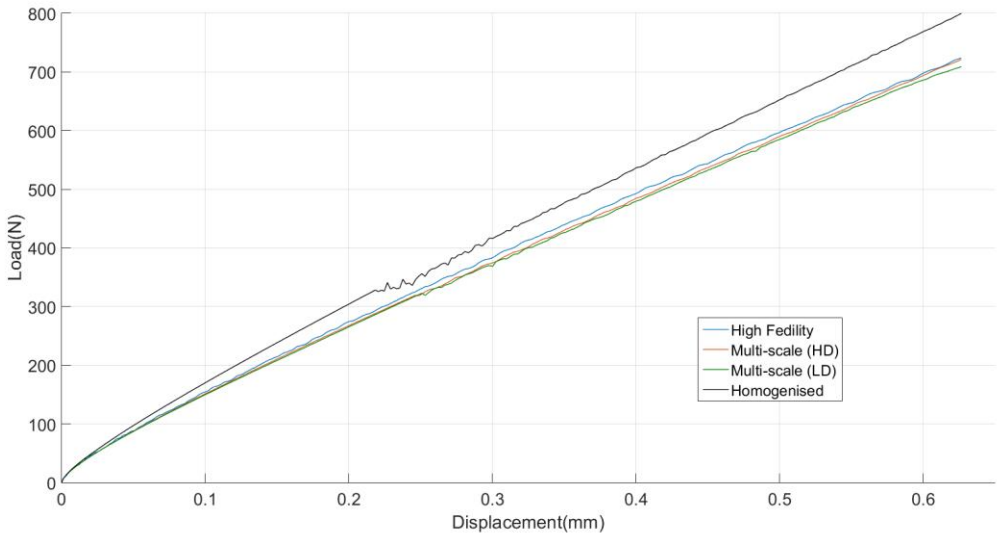

Figure 22 The total force response from the tapered composite model multiscale vs high-fidelity model.

Accepted for publication in Composite Structures, Vol. 200, 15 Sept. 2018, Pages 781-79
https://doi.org/10.1016/j.compstruct.2018.05.078

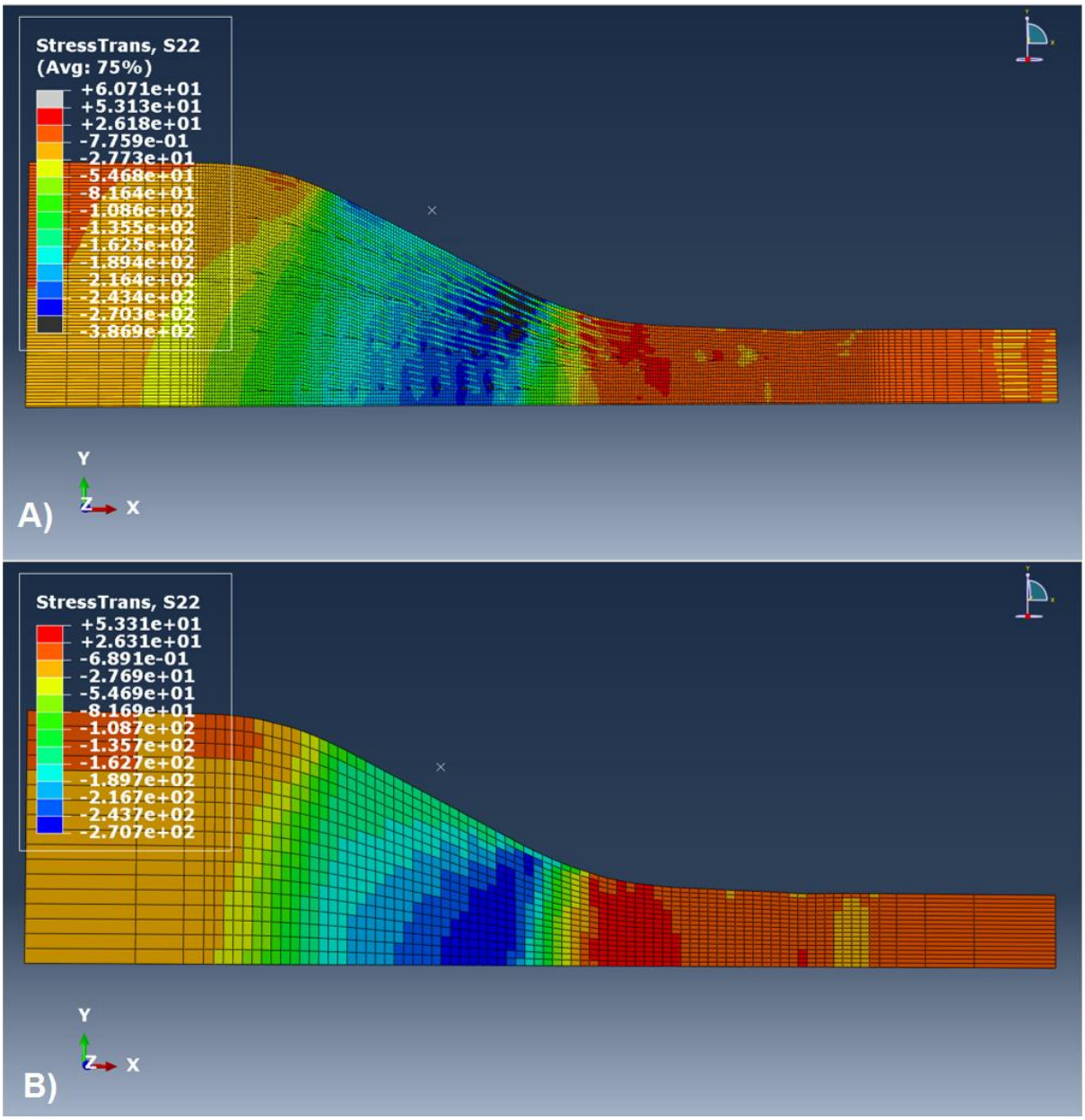

Figure 23 Tapered model through-thickness stress in global coordinates: a) High Fidelity ply by ply model, b) Multi-scale model.

Accepted for publication in Composite Structures, Vol. 200, 15 Sept. 2018, Pages 781-79
https://doi.org/10.1016/j.compstruct.2018.05.078

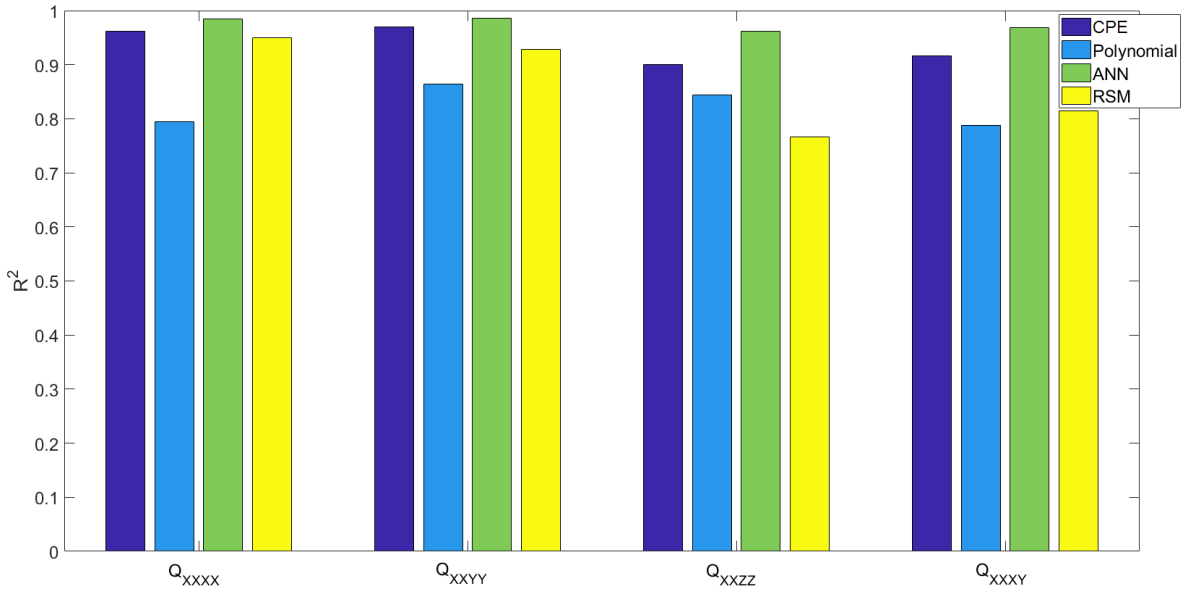

Figure 24 A comparison of the R^2 fit of various surrogate models.

Accepted for publication in Composite Structures, Vol. 200, 15 Sept. 2018, Pages 781-79
https://doi.org/10.1016/j.compstruct.2018.05.078

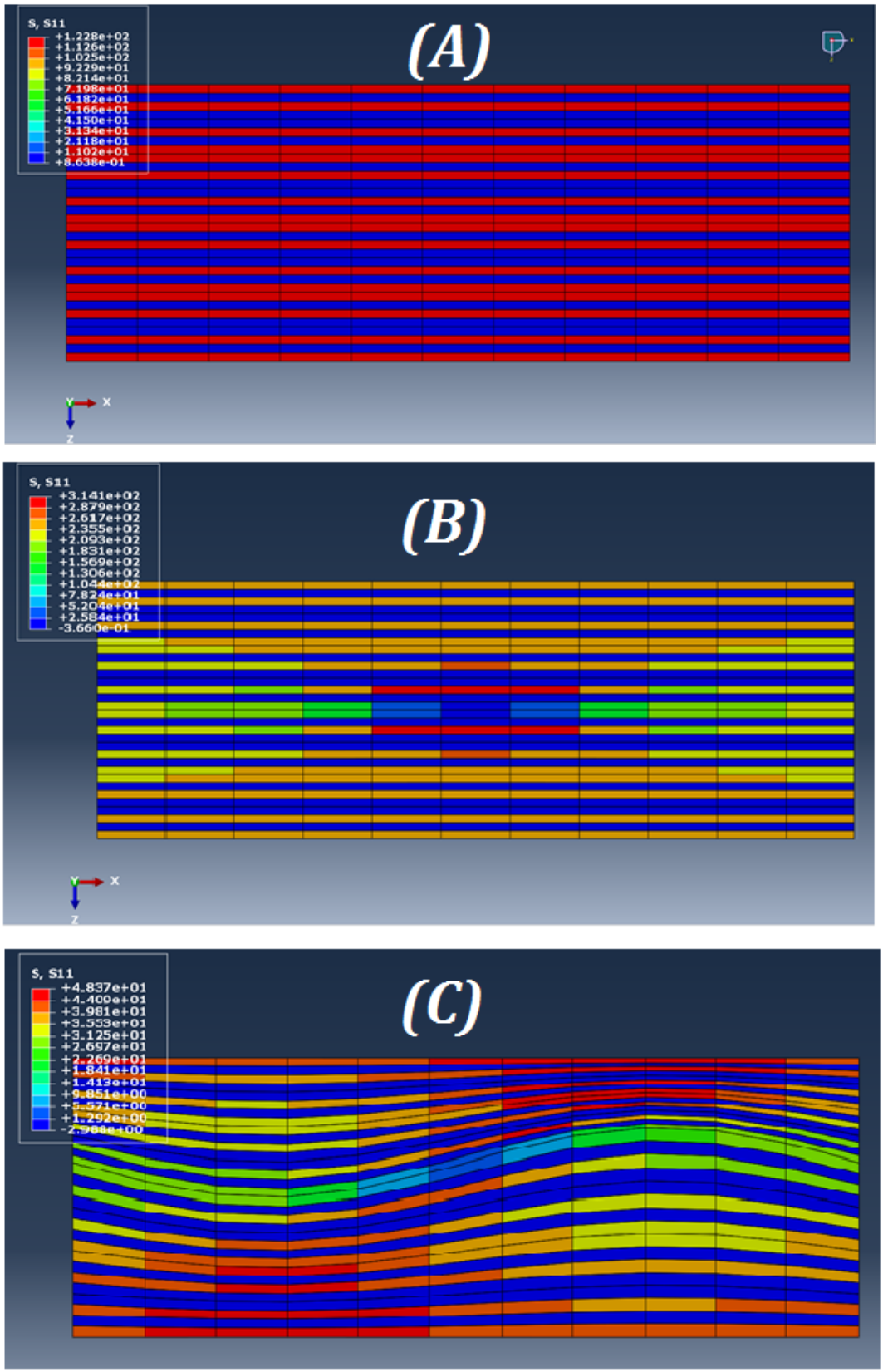

Figure 25 Fibre direction stress of different RVE models. A) Pristine RVE, B) Cut-ply RVE, C) Wrinkle + cut-ply RVE.

Accepted for publication in Composite Structures, Vol. 200, 15 Sept. 2018, Pages 781-79
https://doi.org/10.1016/j.compstruct.2018.05.078

TABLES

Table 1. Surrogate Model Dependencies.

Constant	Lamination Parameters	Number of Fit Constants
$A_{11}, A_{12}, A_{22}, D_{11}$	ζ_1, ζ_2, ω	10
$A_{13}, A_{23}. D_{33}$	ζ_2, ω	5
B_{11}, B_{12}	ζ_3, ζ_4, ω	10
D_{22}, D_{23}	ζ_4, ω	5
A_{33}	Constant	0